AD-A056 199 ILLINOIS UNIV AT URBANA-CHAMPAIGN COORDINATED SCIENCE LAB F/G 9/1
CAPACITIVE TAP WEIGHT NETWORK SURFACE ACOUSTIC WAVE TRANSDUCERS--ETC(U)
MAY 77 D C MALOCHA DAAB-07-72-C-0259
UNCLASSIFIED R-780 NL

1 OF 2
AD
A056199

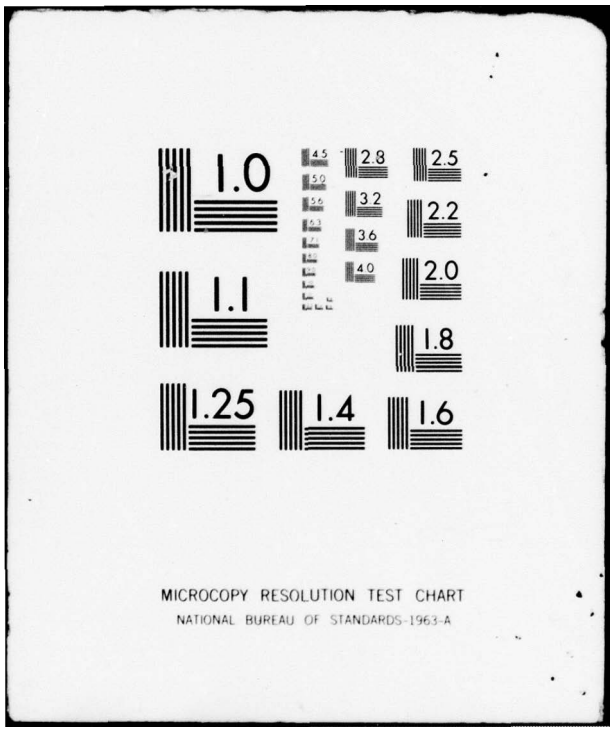
1.0
1.1
1.25
1.4
1.6
1.8
2.0
2.2
2.5
2.8
3.2
3.6
4.0
4.5
5.0
5.6
6.3
MICROCOPY RESOLUTION TEST CHART
NATIONAL BUREAU OF STANDARDS-1963-A

REPORT R-780 MAY, 1978 LEVEL II UILU-ENG 77-2227

CSL COORDINATED SCIENCE LABORATORY

12

CAPACITIVE TAP WEIGHT NETWORK SURFACE ACOUSTIC WAVE TRANSDUCERS

DONALD CHESTER MALOCHA

UNIVERSITY OF ILLINOIS - URBANA, ILLINOIS

UNCLASSIFIED

SECURITY CLASSIFICATION OF THIS PAGE *(When Data Entered)*

REPORT DOCUMENTATION PAGE

READ INSTRUCTIONS BEFORE COMPLETING FORM

1. REPORT NUMBER	2. GOVT ACCESSION NO.
3. RECIPIENT'S CATALOG NUMBER	
4. TITLE *(and Subtitle)*	5. TYPE OF REPORT & PERIOD COVERED
CAPACITIVE TAP WEIGHT NETWORK SURFACE ACOUSTIC WAVE TRANSDUCERS,	Technical Report
6. PERFORMING ORG. REPORT NUMBER	R-780, UILU-ENG-77-2227
7. AUTHOR(s)	8. CONTRACT OR GRANT NUMBER(s)
Donald Chester Malocha	DAAB-07-72-C-0259, F33615-75-C-1291
9. PERFORMING ORGANIZATION NAME AND ADDRESS	10. PROGRAM ELEMENT, PROJECT, TASK AREA & WORK UNIT NUMBERS
Coordinated Science Laboratory University of Illinois at Urbana-Champaign Urbana, Illinois 61801	
11. CONTROLLING OFFICE NAME AND ADDRESS	12. REPORT DATE
Joint Services Electronics Program	May 1977
	13. NUMBER OF PAGES 92 (12) 114 P.
14. MONITORING AGENCY NAME & ADDRESS *(if different from Controlling Office)*	15. SECURITY CLASS. *(of this report)* UNCLASSIFIED
	15a. DECLASSIFICATION/DOWNGRADING SCHEDULE

16. DISTRIBUTION STATEMENT *(of this Report)*

Approved for public release; distribution unlimited

17. DISTRIBUTION STATEMENT *(of the abstract entered in Block 20, if different from Report)*

18. SUPPLEMENTARY NOTES

19. KEY WORDS *(Continue on reverse side if necessary and identify by block number)*

Surface Acoustic Wave

Capacitively Weighted Transducers

20. ABSTRACT *(Continue on reverse side if necessary and identify by block number)*

A new structure for SAW transducer tap weight control using thin film capacitors in a bridge type network has been devised. In the capacitive tap weight network (CTWN), thin film capacitors made with an $SiO_{(x)}$ dielectric are fabricated on each tap in the propagation path so no additional substrate area is used. The impulse response shape is controlled by the voltage attenuation on each finger. This provides a large dynamic range of tap weights without phase variation and a uniform beam width which allows the cascading of two weighted transducers without the use of a multistrip coupler. → next page

DD FORM 1 JAN 73 1473 EDITION OF 1 NOV 65 IS OBSOLETE

UNCLASSIFIED

SECURITY CLASSIFICATION OF THIS PAGE *(When Data Entered)*

20. ABSTRACT (continued)

A model which accurately predicts the multitap CTWN transducer input admittance, insertion loss, thin film losses and electrical Q is presented. Design procedures for capacitive weighted bandpass filters are developed.

Experimental devices with varying designs are presented which verify the CTWN model. The devices presented demonstrate tap weight control, the cascading of weighted transducers, 5 wavelength beam width transducers, tap deletion techniques, general oversampling techniques and inphase-quadrature sampling.

UILU-ENG 77-2227

CAPACITIVE TAP WEIGHT NETWORK SURFACE ACOUSTIC WAVE TRANSDUCERS

by

Donald Chester Malocha

This work was supported in part by the Joint Services Electronics Program (U.S. ARmy, U.S. Navy and U.S. Air Force) under Contract DAAB-07-72-C-0259 and in part by the United States Air Force under Contract F33615-75-C-1291.

CAPACITIVE TAP WEIGHT NETWORK SURFACE ACOUSTIC WAVE TRANSDUCERS

BY

DONALD CHESTER MALOCHA

B.S., University of Illinois, 1972
M.S., University of Illinois, 1974

THESIS

Submitted in partial fulfillment of the requirements
for the degree of Doctor of Philosophy in Electrical Engineering
in the Graduate College of the
University of Illinois at Urbana-Champaign, 1977

Thesis Adviser: Bill J. Hunsinger

Urbana, Illinois

CAPACITIVE TAP WEIGHT NETWORK SURFACE ACOUSTIC WAVE TRANSDUCERS

Donald C. Malocha, Ph.D.
Coordinated Science Laboratory and
Department of Electrical Engineering
University of Illinois at Urbana-Champaign, 1977

A new structure for SAW transducer tap weight control using thin film capacitors in a bridge type network has been devised. In the capacitive tap weight network (CTWN), thin film capacitors made with an SiO_x dielectric are fabricated on each tap in the propagation path so no additional substrate area is used. The impulse response shape is controlled by the voltage attenuation on each finger. This provides a large dynamic range of tap weights without phase variation and a uniform beam width which allows the cascading of two weighted transducers without the use of a multistrip coupler.

A model which accurately predicts the multitap CTWN transducer input admittance, insertion loss, thin film losses and electrical Q is presented. Design procedures for capacitive weighted bandpass filters are developed.

Experimental devices with varying designs are presented which verify the CTWN model. The devices presented demonstrate tap weight control, the cascading of weighted transducers, 5 wavelength beam width transducers, tap deletion techniques, general oversampling techniques and inphase-quadrature sampling.

ACKNOWLEDGMENTS

The author wishes to thank all the members of the SAW group at CSL who contributed either directly or indirectly to this investigation. A special thanks to Steve Wilkus for his assistance in many of the computer programs.

The author wishes to thank Mrs. H. Corray for the excellent job in typing the manuscript.

A very special note of gratitude to Bill Hunsinger who provided direction, lent criticism and provided moral support throughout the course of the investigations. His advice and friendship is greatly appreciated. Finally, the author wishes to thank his wife, Karen, and daughter, Linnette, for their encouragement throughout the course of the project.

TABLE OF CONTENTS

I. INTRODUCTION

Since surface acoustic waves (SAW) emerged in the late 1960's as a means for signal processing in the VHF-UHF range, they have made a major impact in the communication industry. SAW devices are fabricated using the planar technology well established in the semiconductor industry which is responsible, to a large extent, for the rapid development of SAW technology. The review article by Hayes and Hartmann [1] provides an excellent background for the advances made in the surface wave area while including a fairly extensive bibliography for detailed information. Notable achievements have been made in bandpass filters, as indicated in the review article, for obtaining low insertion loss (IL), large sidelobe rejection, low passband ripple and nearly linear phase. However, many of these achievements are not applicable to the general class of bandpass filters and further, the parameters are interleaved in ways that make simultaneous optimization of all the parameters impossible at this time. This dissertation describes a new weighting configuration for the generation of SAW which applies to a large class of bandpass filters and other signal processors where accurate tap weight control is necessary [2,3].

Apodization is the most widely used technique for adjusting the tap weight of surface acoustic wave interdigital transducers (IDT). When an apodized transducer is used to generate SAWs, the amplitude is constant but there is spatial variation of the beam which is directly proportional to the relative tap weight as illustrated in Figure 1a. The major disadvantages of apodization are: 1) it requires a non-apodized input transducer or the use of a multistrip coupler [4], which uniformly distributes

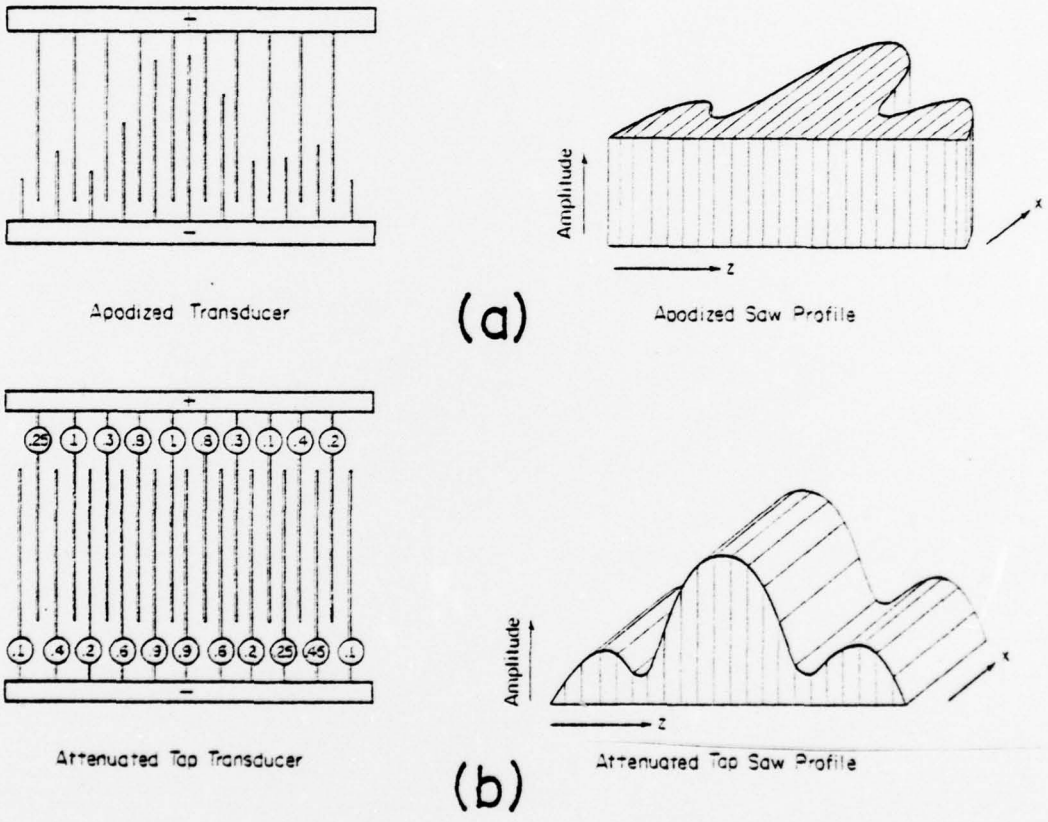

Figure 1. Illustration of typical surface waves having identical sampled impulse responses generated by: a) apodization and b) tap attenuation techniques.

the beam, 2) it is difficult to model because of the varying overlap, 3) it has increased diffraction errors, and 4) it has an inherent loss due to nonuniform interaction across the beam.

As an alternative, tap attenuator techniques control the coupling strength of equal length taps to adjust the time response and produce a constant beam width SAW with varying amplitudes as illustrated in Figure 1b. The advantages gained by having a uniform beam width are:

1) the cascading of two weighted transducers is implemented without a multistrip coupler for better filtering and bulk mode suppression,
2) parasitic capacitance and finger end effects are constant and easily modeled,
3) inherent loss due to non-uniform interaction across the beam is eliminated, and
4) diffraction analysis and compensation have the greatest success for non-apodized transducers since the beam aperature is fixed and electrostatic beam effects occur only at the beam edges [5,6]. A number of techniques for introducing tap attenuation have been used in special applications with varying degrees of success, however, each technique has limitations which prevent its general use.

The capacitive tap weight network (CTWN) transducer discussed in this dissertation uses an attenuator on each individual finger to adjust the applied tap voltage while allowing all electrodes to have the

same length as shown in Figure 1b. The attenuator is realized through the use of thin film capacitors in a bridge type of network, as shown in Figure 2, using well developed fabrication techniques similar to those used in the thin film and integrated circuit industries. The CTWN transducer provides a large dynamic range of tap weights without phase variation and a uniform beam width which allows the cascading of two weighted transducers without the use of a multistrip coupler. The periodicity of the structure and uniform beam width minimizes finger end effects and parasitic capacitance allowing the development of a simple model which accurately predicts the SAW impulse response.

Various attempts have previously been made to obtain tap weight control through the use of voltage attenuation while maintaining a uniform beam width. Tanski [7] introduced a coupling bar to obtain a voltage divider circuit on the acoustic substrate. This technique has not been actively pursued since it requires increased substrate area due to the coupling section, the generation of an undesirable surface wave which must be absorbed while adding device insertion loss, and does not account for the interactions in the coupling section. Rosenfeld, et al. [8] proposed using thin film capacitors in series with the finger electrodes which control the tap amplitudes but introduce tap phase errors. Hunsinger, et al. [9] used a tuning fork technique which breaks the beam into a required number of sections determined by the tap weights. This approaches a uniform beam, however, the taps are limited to only discrete values. Withdrawal weighting, first introduced by Hartmann [10], has proven to be an excellent means of weighting narrowband filters while

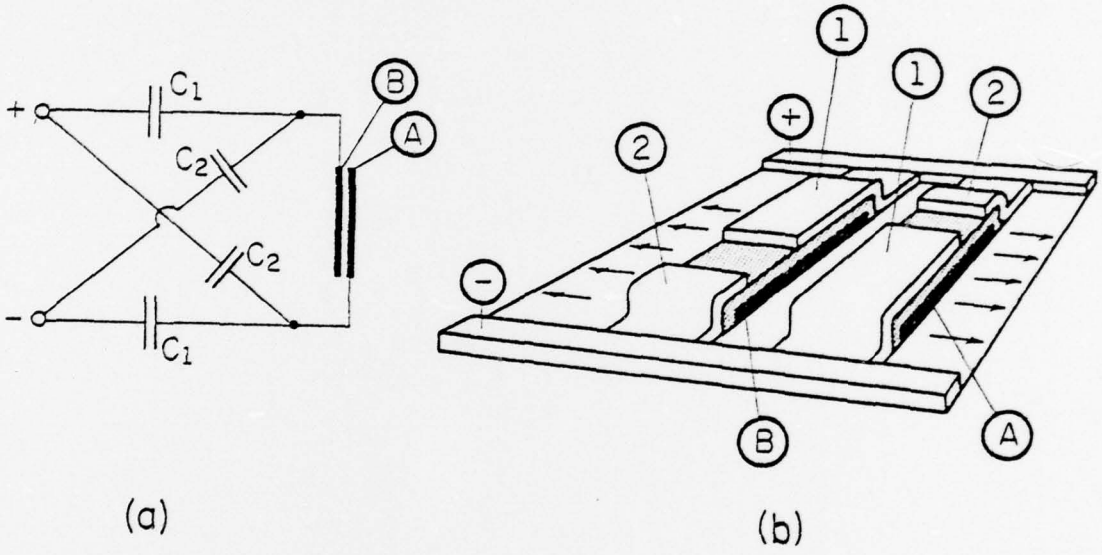

Figure 2. The CTWN bridge for a single finger pair: a) electrical equivalent circuit and b) physical structure.

maintaining a uniform beam. This design works best if the ratio of the largest amplitude to the smallest amplitude in the impulse response weighting envelope is reasonably small which limits its usefulness to narrowband filters where there are many taps.

The CTWN transducer allows dynamic tap weight control without introducing unwanted phase variations. Although attenuators are placed on the substrate, they lie in the propagation path thereby eliminating any increase in substrate area. The weighting is applicable to the general class of bandpass filters with the insertion loss dependent upon the piezoelectric substrate material parameters, thin film dielectric and conductor properties and the percent bandwidth of the device. In general, the CTWN transducer will have an increased electrical Q, with respect to a similar apodized device, which causes increased insertion loss for wideband filters. Accurate tap weight control is maintained since all the thin film capacitors are fabricated under identical conditions in a single evaporation process and the capacitor areas are defined through a single photolithographic mask. Devices will be presented having beam widths of only five wavelengths and yielding accurate filter responses. A complete model, including losses, together with a summary of design procedures are presented. The CTWN transducer adds greater versatility to design and experimental verification of the model using a number of different configurations and sampling techniques is provided.

II. CAPACITIVE TAP WEIGHT NETWORK TRANSDUCER MODEL

There are quite a number of different first order models and design procedures for accurately characterizing a SAW transducer [11, 12, 13, 14, 15] each of which has advantages and disadvantages. Coupled with these first order models are second order analysis which discuss MEL and regenerative wave distortion, tap interactions, end effects, triple transit echos and matching [16, 17, 18, 5, 6]. The approach used to characterize a filter is to first accurately define the first order model and then use a superposition of second order models to predict second order distortion effects and eliminate or minimize these distortions.

This section will discuss the first order analysis of CTWN transducers. The impulse response model [13] will be developed since it is the most widely used and accurately predicts the parameters needed for SAW design. A multi-element model and loss analysis are provided for complete design capability. Experimental verification of the model is provided in Section III and second order effects are discussed where applicable.

A. Single Tap Analysis

The CTWN structure for a single isolated tap, as shown in Figure 2, consists of finger lines labeled A and B deposited directly on the piezoelectric substrate, a dielectric layer, and upper electrodes labeled 1 and 2 . The signal is placed across the buss bars of the upper layer and is capacitively coupled to the lower finger pair which generates a a surface wave. The coupling strength is dependent upon the difference of capacities C_1 and C_2 and their relative values with respect to the

finger pair capacitance. This structure allows the transducer size to remain constant with varying weight. Figure 3 is the simplified equivalent electrical circuit of the CTWN structure using the standard IDT cross field model [19] for the finger pair.

The sum of the series capacitor, C_1, and shunt capacitor, C_2, is defined as the bridge attenuator capacitance

$$C_T = C_1 + C_2 \tag{A-1}$$

and the transducer capacitance, C_s, established by the lower finger lines and the piezoelectric substrate is similar to the capacity of the ID transducer. The ratio of the transducer capacitance to the bridge attenuator capacitance is defined as the transducer bridge reactance ratio

$$\alpha_R = C_s/C_T = \frac{C_s}{C_1 + C_2} \tag{A-2}$$

The ratio of the differential capacitance

$$\Delta C = C_1 - C_2$$

to the bridge attenuator capacitance is defined as the attenuator gain

$$\alpha_w = \frac{C_1 - C_2}{C_1 + C_2} = \Delta C/C_T \tag{A-3}$$

For C_2 equal zero, the attenuator gain is maximum and when $C_2 = C_1$, it is 0. The dynamic range is determined by the capacitor balance which is very accurately set with I.C. technology. With $Z_o = 1$, the turns ratio in the cross field model for an electrode pair is the familiar expression [19]

$$r^2 = 4\pi^{-1}\,\omega\, C_s k^2 \tag{A-4}$$

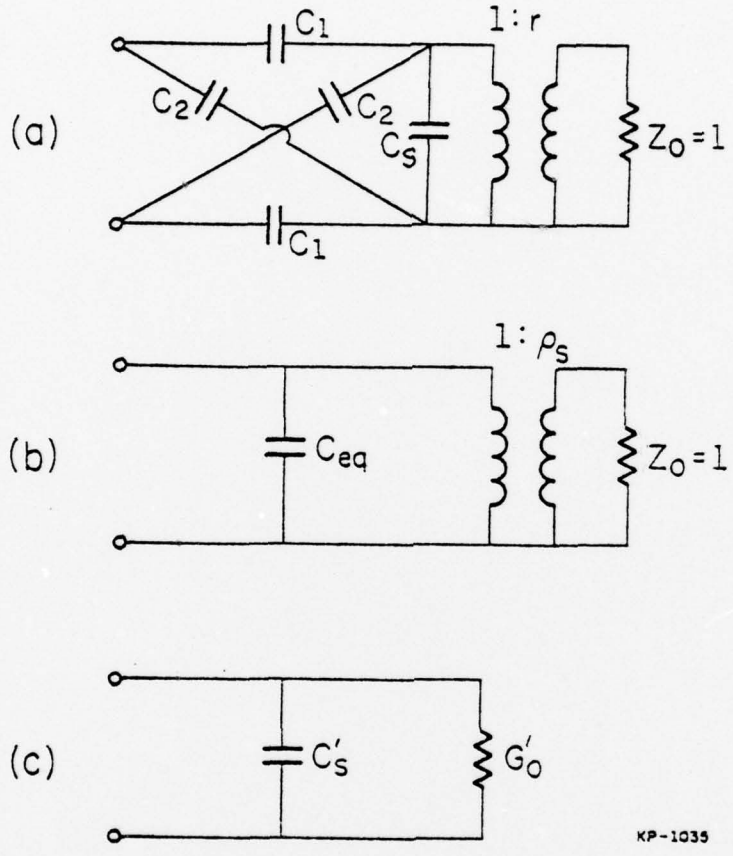

Figure 3. The CTWN equivalent electrical circuits. a) The thin film bridge network with the IDT cross field model for the finger pair. b) Reduction of circuit to an equivalent capacitor and a reduced turns ratio. c) Reduced equivalent circuit representing a CTWN single tap.

The acoustic radiation conductance for a single isolated lower finger pair which is nearly constant near center frequency is given by

$$G_o = r^2/Z_o = 4\pi^{-1}\,\omega\, C_s k^2 \qquad *(A\text{-}5)$$

The CTWN bridge network is considered a two port network with the equivalent circuit for the interdigital electrode pair being the load. The attenuator transfer function is

$$|A(\omega)| = \frac{\omega(C_1 - C_2)}{\sqrt{\omega^2 (C_1 + C_2 + 2C_s)^2 + 4G_o^2}} \qquad (A\text{-}6)$$

$$\arg\underline{/A(\omega)} = \frac{2G_o}{\omega(C_1 + C_2 + 2C_s)}$$

Using substitutions with equations (A-2), (A-3), and (A-5) the attenuator transfer function, which is independent of frequency, is written as

$$|A(\omega)| = |A_o| = \frac{\alpha_w}{\sqrt{(1 + 2\alpha_R)^2 + 64\pi^{-2}k^4\alpha_R^2}} \qquad (A\text{-}7)$$

$$\arg\underline{/A(\omega)} = \arg\underline{/A_o} = \frac{8\pi^{-1}k^2\alpha_R}{(1 + 2\alpha_R)} \,.$$

For a given piezoelectric coupling coefficient (k^2), the denominator of $|A_o|$ is a function of α_R and defined as

---

*k^2 is the coupling coefficient including the effect of the dielectric film.

$$K^{-1} = \frac{1}{\sqrt{4(1+16\pi^{-2}k^4)\alpha_R^2 + 4\alpha_R + 1}} .$$

For YZ LiN_bO_3, $16\pi^{-2}k^4 = 3.43 \times 10^{-3}$ and for ST quartz, $16\pi^{-2}k^4 = 7.85 \times 10^{-6}$. It can be concluded that in most cases K is:

$$K \approx \frac{1}{(1+2\alpha_R)} \qquad \text{(A-8)}$$

and K^2 versus α_R is plotted in Figure 4. The parameter K^2 is interpreted as a capacitive coupling coefficient of the composite tap because it defines the mutual stored energy between the thin film capacitors and the finger capacitance with an attenuator gain of 1. The ability to control this parameter is an important feature of the CTWN.

The attenuator transfer ratio reduces to

$$|A_o| = \alpha_w K . \qquad \text{(A-9)}$$

Examining equation (A-9) shows that so long as K remains constant, the attenuator gain (which is linearly dependent on ΔC) is the normalized tap weight. The restraint that K remain constant (which implies α_R is constant) yields tap weight control without phase variation which is an important criterion for simplifying filter design. This criterion is not met in the series capacitive weighted approach where a single capacitor is in series with the acoustic finger capacitance [8]. For the series weighted transducer ($C_2 = 0$) the tap weight is controlled by the ratio of coupling capacitance to finger impedance but the attenuator argument also varies with tap weight which cause loss of selectivity in the filter response. Attenuator phase shift as calculated from equation (A-7) with $C_2 = 0$ is plotted in Figure 5. For low coupling coefficient

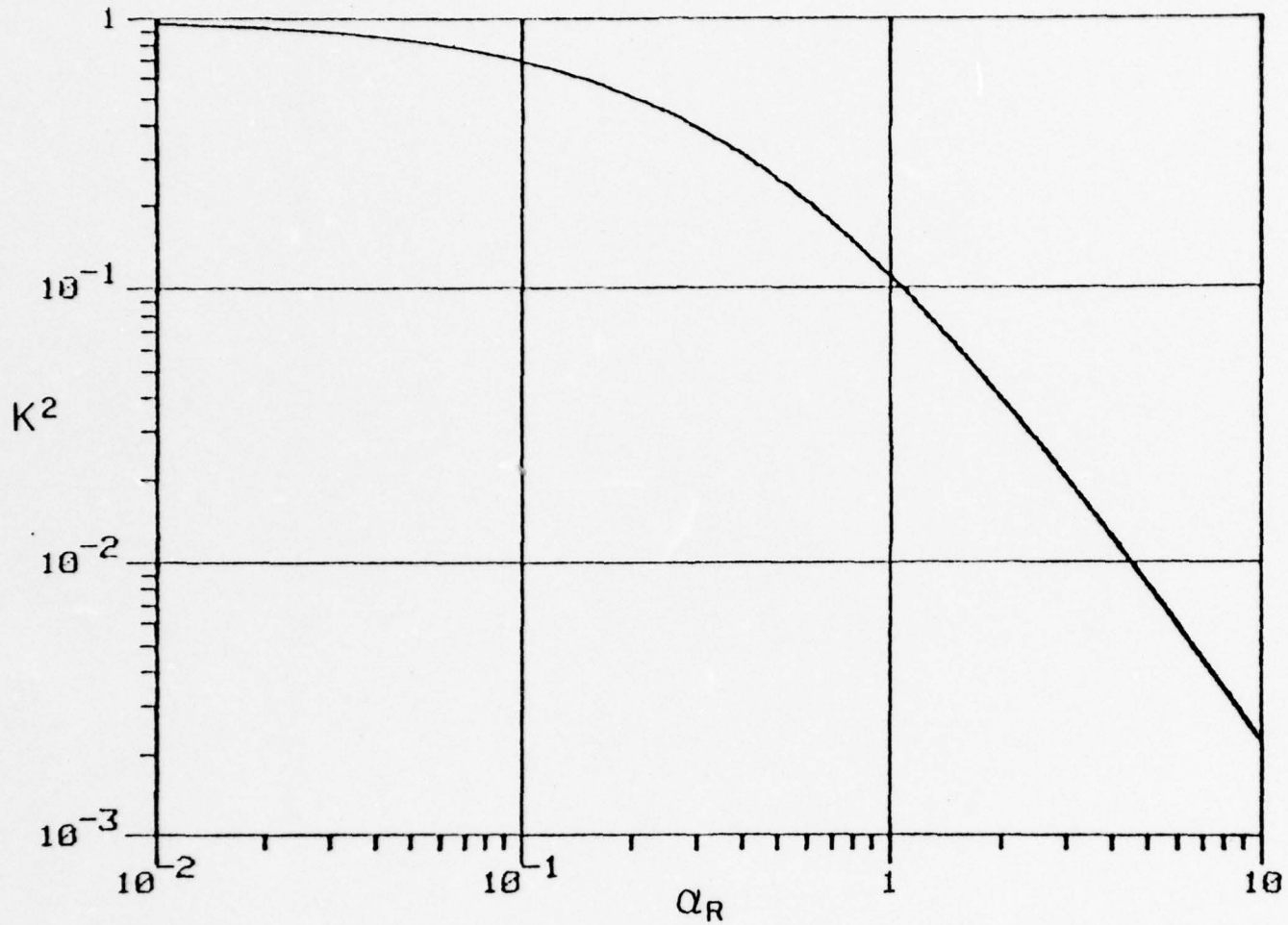

Figure 4. Capacitive coupling coefficient versus the transducer bridge reactance ratio.

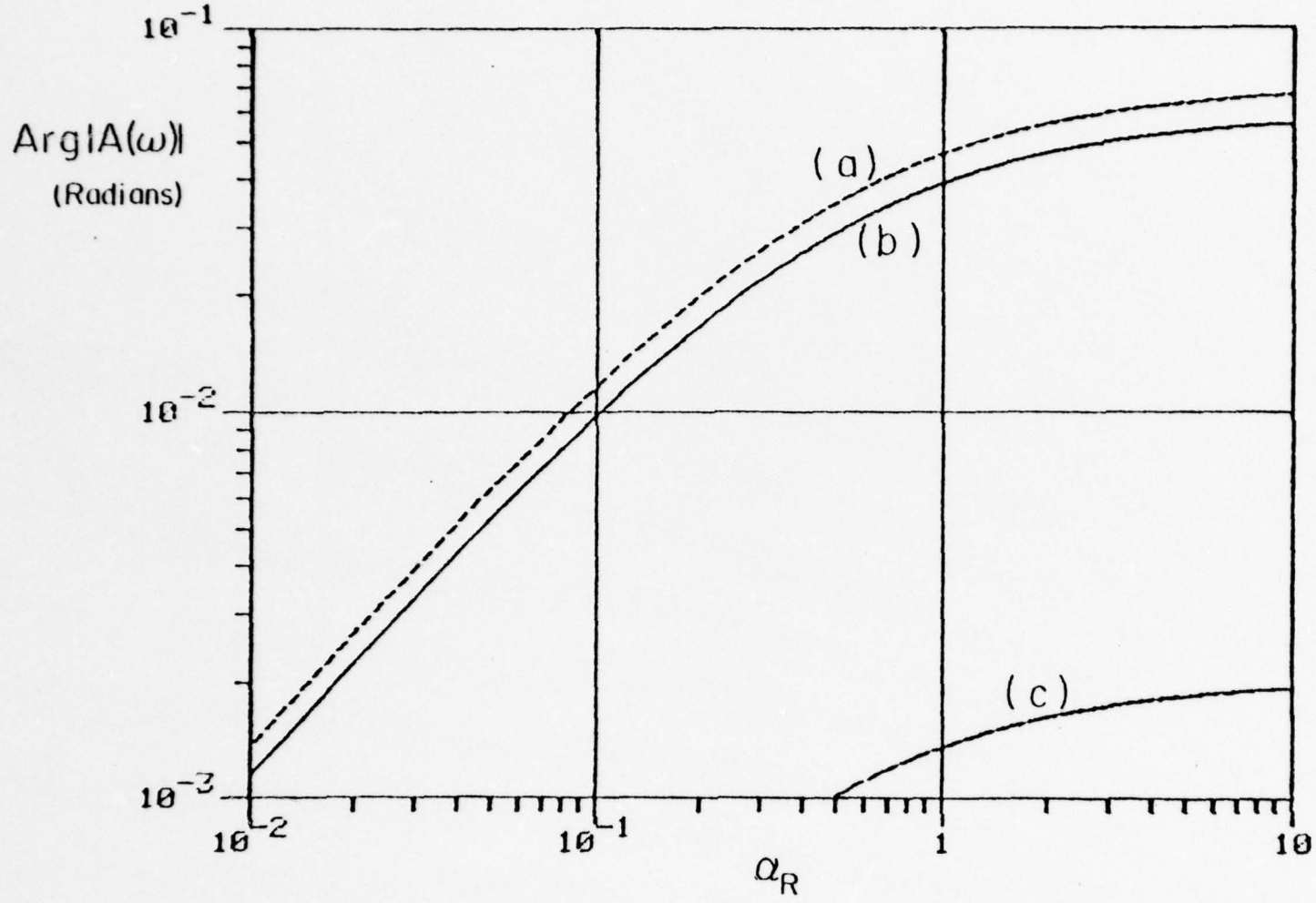

Figure 5. The argument of the attenuator transfer ratio versus the transducer bridge reactance ratio: a)128° YX $LiNbO_3$, b) YZ $LiNbO_3$, and c) ST Quartz.

materials such as ST Quartz, tap phase errors are small while for larger coupling coefficient materials such as YZ $LiNbO_3$, tap phase varies significantly with α_R and must be considered if α_R is allowed to vary.

The acoustic conductance of a single tap is given by

$$G_o' = \frac{\omega^2 (C_1 - C_2)^2 r^2}{\omega^2 (C_1 + C_2 + 2C_s)^2 + 4G_o^2}$$

and upon substituting in equations (A-2), (A-3), and (A-5) the simplified expression is

$$G_o' = \alpha_w^2 K^2 r^2 \ . \qquad \text{(A-10)}$$

The effective turns ratio is reduced from r to $r\rho_s$ where

$$\rho_s = K\alpha_w \ . \qquad \text{(A-11)}$$

Since α_w is the attenuator gain, K^2 effectively reduces the coupling coefficient for unity gain and the maximum coupling coefficient using a CTWN transducer is $k^2 K^2$. This added dimension allows the designer to choose the coupling coefficient which best suits his design criteria (i.e., it is possible to choose a reduced coupling coefficient for long time delay transducers).

The input capacitance is

$$C_s' = \frac{[2G_o^2 (C_1 + C_2) + \omega^2 (C_1 + C_2 + 2C_s)(C_1 C_s + C_2 C_s + 2C_1 C_2)]}{4G_o^2 + \omega^2 (C_1 + C_2 + 2C_s)^2}$$

Substituting equations (A-2), (A-3), and (A-4) one obtains

$$C_s' = \left[1 - \frac{\alpha_w^2}{(1+2\alpha_R)}\right] \frac{C_s}{2\alpha_R} \qquad \text{(A-12)}$$

The minimum value of $C_s'(\alpha_w)$ occurs when the attenuator gain is one and the maximum value occurs when it is zero

$$C_s'(\text{min}) = C_s'(1) = \left[1 - \frac{1}{(1+2\alpha_R)}\right] C_s/2\alpha_R \qquad \text{(A-13)}$$

$$C_s'(\text{max}) = C_s'(0) = C_s/2\alpha_R \ .$$

Figure 6 plots the family of curves for C_s'/C_s versus attenuator gain with the transducer bridge reactance ratio as a parameter. The normalized capacitance (C_s'/C_s) remains nearly constant for tap weights in the range from .001 to .1 and the maximum capacitance is inversely proportional to the transducer bridge reactance ratio. In an apodized transducer most of the input capacitance is due to the large taps, however, small taps in the CTWN actually have a greater input capacitance and the total CWTN transducer capacitance becomes larger if a greater number of small taps are required.

B. Multitap Transducer Analysis Using the Impulse Response Model

The impulse response model as described by Hartmann, et al.[13] provides easy computation of the first order SAW filter response for IDT. The following analysis applies the IR model to the CTWN and derives the equivalent circuit parameters shown in Figure 7. The input admittance of an arbitrary CTWN transducer is obtained by using conservation of energy, where it is assumed that all the energy is dissipated in the

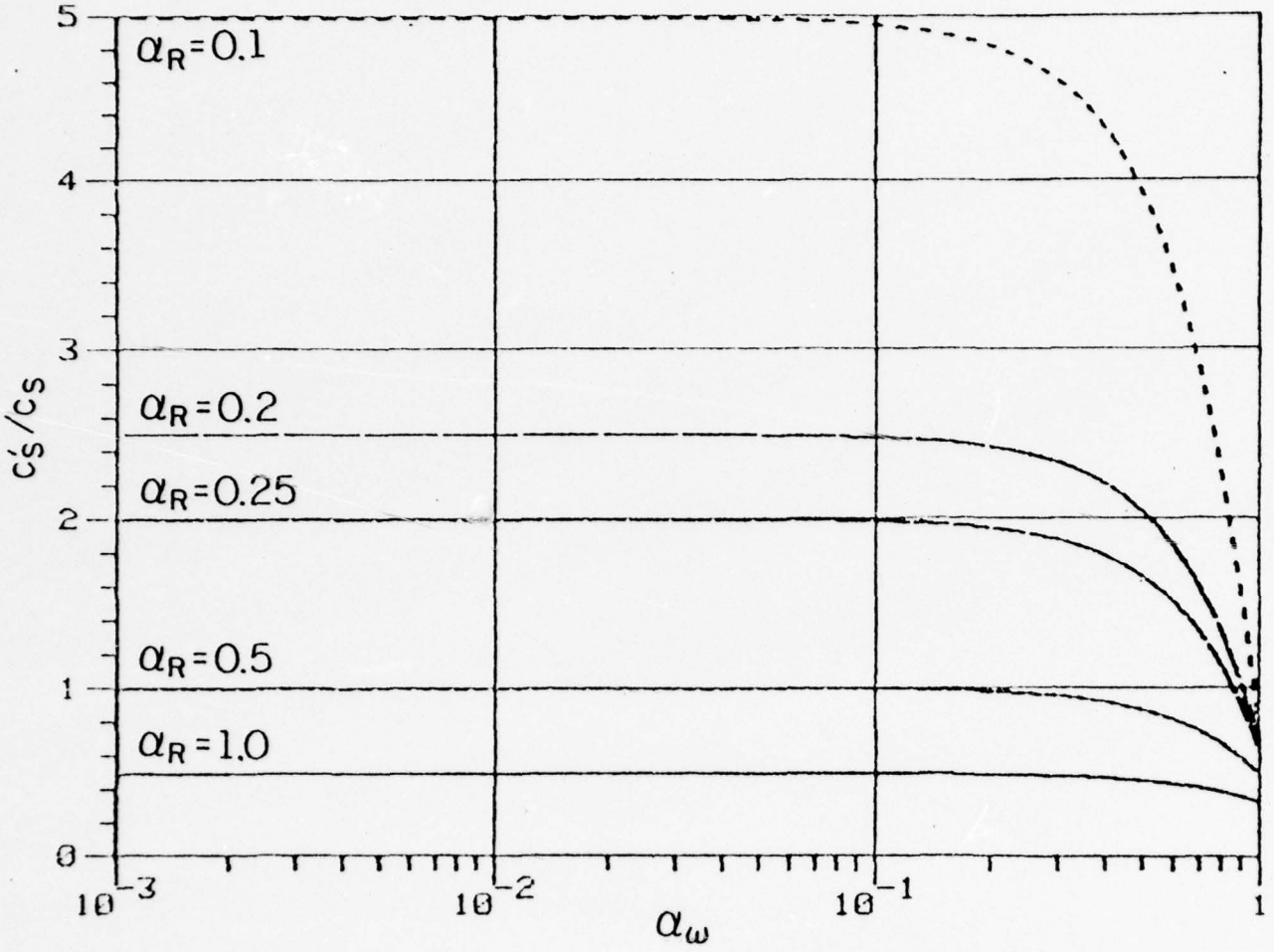

Figure 6. Normalized tap capacitance versus the attenuation gain with the transducer bridge reactance ratio as a parameter.

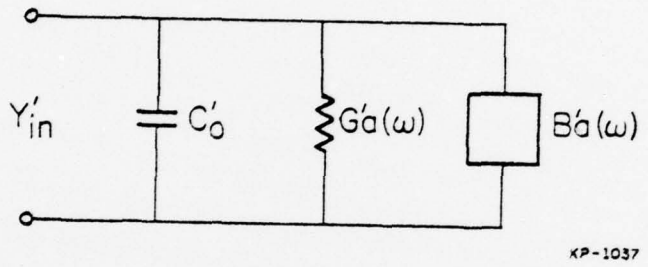

Figure 7. Equivalent circuit for the input admittance of a CTWN transducer.

acoustic conductance. The Fourier transform of the transducer impulse response h(t) yields the corresponding transducer frequency response H(ω). The energy radiated from the acoustic ports of a transducer with time duration τ when driven by an impulse response is

$$E(\omega) = H(\omega)\cdot H^*_{(\omega)} + H^*_{(\omega)} e^{-j\omega T}\cdot H_{(\omega)} e^{j\omega T} = 2\left|H(\omega)\right|^2$$

From Figure 7 this same energy must be dissipated through the acoustic conductance $G'_a(\omega)$ with the relation

$$E(\omega) = V^2_{IN}(\omega) G'_a(\omega) \qquad \text{(B-1)}$$

For $V_{IN}(\omega) = 1$, this is simply

$$G'_a(\omega) = E(\omega) = 2\left|H(\omega)\right|^2 \qquad \text{(B-2)}$$

Since this is a causal system, the susceptance is found through the Hilbert transform yielding

$$B'_a(\omega) = \frac{1}{\pi} \int_{-\infty}^{\infty} \frac{G'_a(\omega')}{\omega'-\omega}\, d\omega' \ .$$

There is also the static capacitance of the electrodes which is found by using equation (A-12) and summing for all the electrodes in the array. This defines all the elements of the electrical input admittance for the CTWN transducer.

1). Input Admittance for Non-Weighted Non-Dispersive Filters

The impulse response of a N pair non-weighted transducer is [13]

$$h(t) = f_o^{3/2} 4k \sqrt{C_s} \sin \omega_o t \qquad 0 \leq t \leq N/f \tag{B-3}$$

$$= 0 \qquad t < 0, \frac{N}{f_o} < t$$

and

$$H(\omega) \cong 2k \sqrt{C_s f_o} N[(\sin X)/X] e^{-j\omega N/2f_o} \tag{B-4}$$

where $X = N\pi(\omega - \omega_o)/\omega_o$. The acoustic radiation admittance parameters are

$$G_a(\omega) = G_a(\omega_o) \frac{\sin^2 X}{X^2} \tag{B-5}$$

where $G_a(\omega_o) = 8k^2 C_s f_o N^2$. Use of the Hilbert transform yields

$$B_a(\omega) = \frac{G_a(\omega_o)[(\sin 2X) - 2X]}{2X^2} \tag{B-6}$$

At center frequency $B_a(\omega_o) = 0$, therefore the reactance is due only to the static capacitance C_o.

The above analysis is applicable to the CTWN when making simple changes in variable. The bridge network introduces a capacitive coupling coefficient so that the reduced acoustic conductance for the CTWN structure at center frequency becomes

$$G'_a(\omega_o) = 4\pi^{-1} \omega_o k^2 K^2 \alpha_w^2 C_s N^2 \tag{B-7}$$

For the specific example of a non-weighted transducer, the acoustic conductance varies depending on the choice of K^2 and α_w^2 for all taps. The static capacitance of a CTWN transducer is given by

$$C_o' = \frac{NC_s}{2\alpha_R}\left[1 - \frac{\alpha_w^2}{1+2\alpha_R}\right] \qquad \text{(B-8)}$$

In an overlap structure, the ratio of C_o to G_o remains constant with respect to beam width, therefore the Q is only dependent on N, the number of taps. However, in the CTWN transducer the ratio of C_o' to $G_a'(\omega_o)$ is dependent on N and the choice of α_R and α_w. The electrical radiation Q of the CTWN transducer at center frequency is defined as

$$Q_R' = \frac{\omega_o C_o'}{G_a'(\omega_o)} \qquad \text{(B-9)}$$

Using equations (B-7) and (B-8) this is rewritten as

$$Q_R' = \frac{\pi}{4k^2N}\left[\frac{1 - \frac{\alpha_w^2}{1+2\alpha_R}}{K^2 2\alpha_R \alpha_w^2}\right] \qquad \text{(B-10)}$$

For the constant overlap IDT structure the Q is defined as

$$Q_R = \frac{\pi}{4k^2N} \qquad \text{(B-11)}$$

The Q enhancement ratio is defined as the CTWN Q divided by the IDT Q

$$\frac{Q_R'}{Q_R} = \left[\frac{1 - \frac{\alpha_w^2}{1+2\alpha_R}}{K^2 2\alpha_R \alpha_w^2}\right] \qquad \text{(B-12)}$$

There is a minimum value for the Q enhancement ratio with a proper choice of the bridge reactance ratio. This is found by taking the derivative of Q_R'/Q_R with respect to α_R and setting the result equal to zero, which yields

$$\frac{\delta (Q_R'/Q_R)}{\delta \alpha_R} = \left[\frac{4\alpha_R^2 + (\alpha_w^2 - 1)}{2\alpha_w^2 \alpha_R} \right] = 0 \qquad \text{(B-13)}$$

therefore, the minimum Q enhancement occurs when

$$\alpha_R = \frac{\sqrt{1-\alpha_w^2}}{2} \qquad \text{(B-14)}$$

If a reduced coupling coefficient is necessary, the Q enhancement ratio is set by choosing appropriate values of α_R and α_w. The Q enhancement ratio is plotted in Figure 8 versus the transducer bridge reactance ratio with attenuator gain as a parameter.

2). Input Admittance for Weighted CTWN Transducer

The following extends the non-weighted transducer analysis to the weighted and compares the results to that of an apodized transducer. The acoustic conductance, $G_a(\omega)$, of an apodized transducer having an impulse response h(t) from equation (15) is approximately

$$G_a(\omega) = 2|H(\omega)|^2$$

where

$$H(\omega) = \text{F.T.}\{h(t)\} .$$

Therefore, the acoustic conductance is expanded as [13]

$$G_a(\omega) \approx 4\pi^{-1} \omega_o C_s k^2 |\text{F.T.}\{w(t)\}|^2 \qquad \text{(B-15)}$$

where w(t) is the sampled impulse response corresponding to the finger overlaps and position. The acoustic conductance of a CTWN transducer is

$$G_a'(\omega) = 4k^2K^2 \pi^{-1} \omega_o C_s \left| \{ \sum_{n=1}^{N} \alpha_w(n) e^{j\omega T} \} \right|^2 \qquad \text{(B-16)}$$

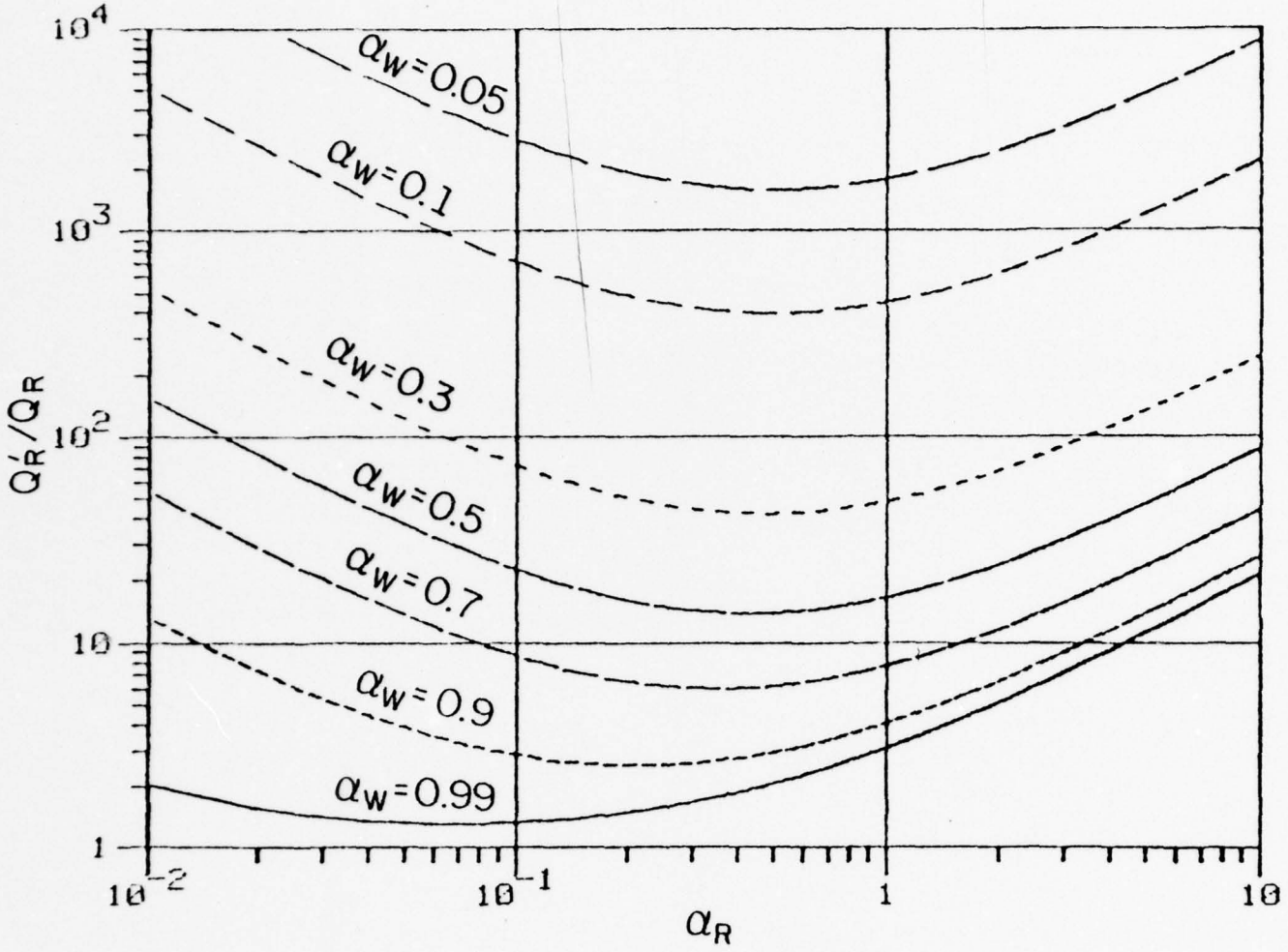

Figure 8. The Q enhancement ratio versus the transducer bridge reactance ratio with the attenuator gain as a parameter.

where the bracketed term is the Fourier transform of the tap weights which correspond to the desired impulse response. For uniform sampling the acoustic conductance at center frequency is given by

$$G'_a(\omega_o) = 4k^2K^2\pi^{-1}\omega_o C_s \left| \sum_{n=1}^{N} \alpha_w(n)\, e^{j\omega_o \tau n} \right|^2 \qquad \text{(B-17)}$$

or

$$G_a(\omega_o) = 4k^2K^2\pi^{-1}\omega_o C_s N_{eff}^2$$

where $N_{eff} = \sum_{n=1}^{N} \alpha_w(n)\, e^{j\omega_o \tau_o n}$, N is the number of taps, and τ_o corresponds to the delay between electrodes. For a uniform sampled device where $\tau_o = 1/2\ f_o$ and having no time sidelobes, N_{eff} is simple

$$N_{eff} = \Sigma\ (-1)^n\ \alpha_w(n)\ . \qquad \text{(B-18)}$$

The CTWN input capacitance is the sum of the individual tap capacitances from equation (A-12)

$$C'_o = \sum_{n=1}^{N} \left[1 - \frac{\alpha_w^2(n)}{(1+2\alpha_R)}\right] \frac{C_s}{2\alpha_R}$$

or

$$C'_o = \frac{NC_s}{2\alpha_R} \left[1 - \frac{\overline{\alpha_w^2}}{(1+2\alpha_R)}\right] \qquad \text{(B-19)}$$

where $\overline{\alpha_w^2}$ equals the average squared tap weight value. The input capacitance for a similar apodized device is approximately

$$C_o = \sum_{n=1}^{N} \alpha_w(n)\ C_s = \overline{\alpha_w}\ NC_s \qquad \text{(B-20)}$$

where $\overline{\alpha_w}$ is the average tap weight value. The CTWN transducer introduces additional capacitance to the device over an apodized transducer dependent on the average squared tap weight value. The Q for the CTWN trans-

ducer is defined as

$$Q_R' = \frac{\omega_o C_o'}{G_a'(\omega_o)} = \frac{\frac{\omega_o N C_s}{2\alpha_R}\left[1 - \frac{\overline{\alpha_w^2}}{1+2\alpha_R}\right]}{4k^2K^2\pi^{-1}\omega_o C_s N_{eff}^2} \tag{B-21}$$

$$Q_R' = \frac{\pi}{4k^2}\frac{(1+2\alpha_R)^2}{2\alpha_R}\frac{N}{N_{eff}^2}\left[1 - \frac{\overline{\alpha_w^2}}{(1+2\alpha_R)}\right]$$

The minimum Q is found by taking the derivative of Q_R' and setting the result to zero which yields

$$\frac{\delta Q_R'}{\delta \alpha_R} = \frac{\pi}{4k^2}\frac{N}{N_{eff}^2}\left[\frac{4\alpha_R^2 + \overline{\alpha_w^2} - 1}{2\alpha_R^2}\right] = 0 \tag{B-22}$$

For a given set of tap weights, the minimum Q_R' attainable occurs when:

$$\alpha_{R\ min} = \frac{\sqrt{1 - \overline{\alpha_w^2}}}{2} \tag{B-23}$$

which yields

$$\alpha_{R\ min} = 0 \quad \text{for} \quad \overline{\alpha_w^2} = 1$$

and

$$\alpha_{R\ min} = .5 \quad \text{for} \quad \overline{\alpha_w^2} = 0$$

For most filter applications this sets the desirable range of α_R as

$$0 < \alpha_R < .5$$

For broadband high shape factor filters, α_R is approximately .5, while for narrowband filters α_R will decrease. It is obvious that for the case of a non-weighted impulse response, the interdigital transducer should be used unless a scaling of the effective coupling coefficient or an increased Q is desired.

For filter synthesis it is desirable to convert equation (B-21) into parameters which relate directly to frequency filter specifications. This is done by making substitutions of variables with suitable approximations. Assume a filter having 60 db sidelobe rejection (this restriction is necessary to confine the majority of the energy in the passband), a center frequency of f_o, a 3 db bandwidth of Δf and a transition bandwidth, defined as the bandwidth from the 3 db to 40 db level, TBW. This design is accomplished using an eigen syntheses technique [20]. The transducer has a delay τ and is uniformly sampled with $\Delta t = 1/2\ f_o$ for the delay between samples. For an N tap transducer (2N electrodes), the time delay is written as

$$\tau = N/f_o \tag{B-24}$$

However, the total delay time is also related to the transition bandwidth by [20]

$$\tau \approx 2/TBW \tag{B-25}$$

therefore, equating equation (B-24) to (B-25) yields

$$N = 2f_o/TBW \tag{B-26}$$

The effective number of taps is inversely proportional to the device bandwidth as [13]

$$N_{eff} = f_o/\Delta f \tag{B-27}$$

which is a good approximation to equation (B-18). An estimate of the mean squared tap weight for a raised cosine weighting function is

$$\overline{\alpha_w^2} \approx \frac{\Delta f_{40\ db}}{f_o} \tag{B-28}$$

and will be scaled for other types of weighting functions.

Defining the filter shape factor as

$$S = \frac{\Delta f_{40\ db}}{\Delta f_{3\ db}} = \frac{\Delta f + 2TBW}{\Delta f} \qquad \text{(B-29)}$$

gives a measure of the filter selectivity adjacent to the passband. When S = 3, the transition bandwidth equals the 3 db bandwidth while S= 1 is a perfect square wall filter with no transition bandwidth. For filters having shape factors in the range from 1.3 to 3, equations (B-26) and (B-29) set the approximate mean square tap weight range as

$$.1 < \overline{\alpha_w^2} < .33$$

This range is applicable to an eigen synthesis or other equivalent design synthesis where the sidelobe rejection is approximately 60 db. As the sidelobe level is allowed to be raised, the average squared tap weight value increases and the previous equations have to be modified to account for the increased energy in the sidelobes.

With the filter shape factor limits as $1.3 < S < 3$, the α_R range is

$$.41 \leq \alpha_R \leq .47$$

which is a narrow range. This indicates that the minimum Q_R' is nearly independent of α_R and a value of $\alpha_R = .45$ yields representative results.

Q_R' derived in equation (B-21) is approximated using substitutions of equations (B-26), (B-27), (B-28), and (B-29) as

$$Q_R' \approx \left(\frac{\pi}{4k^2}\frac{\Delta f}{f_o}\right)\left(\frac{16 - 8.48\,\frac{\Delta f}{f_o}}{S-1}\right) \quad \text{for } \alpha_R = .45 \qquad \text{(B-30)}$$

For ease in electrical impedance matching across the entire passband it is required that $Q_R' \leq f_o/\Delta f$. Equation (B-30) is rewritten as

$$8.48\left(\frac{\Delta f}{f_o}\right)^3 - 16\left(\frac{\Delta f}{f_o}\right)^2 + \frac{4k^2}{\pi}(S-1) = 0 \qquad \text{(B-31)}$$

and is used to calculate the single transducer insertion loss versus the percent bandwidth for various shape factors. This approximates the largest fractional bandwidth for a given shape factor where the only loss will be the 3 db bidirectional loss. For larger fractional bandwidths than that calculated in equation (B-31), resistance must be added to the matching circuit to lower the Q with a resulting increase in insertion loss of approximately 12 db per octave of bandwidth.

If the sidelobe level is raised from 60 db to 40 db, the transducer insertion loss is decreased. It is shown that for a Dolph Chebyshev window function, the minimum impulse response length is approximately [13]

$$\tau_{min} = .73/TBW \log R$$

where R is the sidelobe rejection level. This indicates Q_R' for a 40 db sidelobe rejection filter is about 1.5 times smaller than for a filter with 60 db sidelobe rejection with a corresponding reduction in insertion loss. If two transducers are cascaded, the total filter response will still theoretically have 80 db sidelobe rejection which is more than adequate for the majority of filter specifications.

C. Tap Weight Determination in a Multi-element Transducer

The simplified circuit model for a semi-infinite periodic CTWN transducer is shown in Figure 9. The admittance of the lower electrodes is represented by Y_s which is the acoustic admittance including effects at the end of the aperture. Because of the periodicity, every electrode has exactly the same admittance which greatly simplifies the model. Although stray capacitance to ground of the lower electrodes is neglected, this is constant for every electrode and is added as a perturbation on the finger capacitance. The admittances Y_{1i} and Y_{2i} represent the thin film bridge networks fabricated on the device where $Y_{1i} = j\omega C_{1i}$ and $Y_{2i} = j\omega C_{2i}$. As previously mentioned, the constraint for constant α_R is applied which requires

$$C_{1i} + C_{2i} = C_T \tag{C-1}$$

The voltage on the $i^{\underline{th}}$ node is

$$V_i = \frac{Y_s(V_{i+1} + V_{i-1}) + Y_{1i}\, V_o}{Y_{1i} + Y_{2i} + 2Y_s} \tag{C-2}$$

and upon substituting equation (C-1) becomes

$$V_i = \frac{Y_s(V_{i+1} + V_{i-1}) + Y_{1i}\, V_o}{Y_T + 2Y_s} \tag{C-3}$$

The $i^{\underline{th}}$ tap weight is defined as

$$TW_i = V_i - V_{i+1} \tag{C-4}$$

which using equation (C-3) becomes

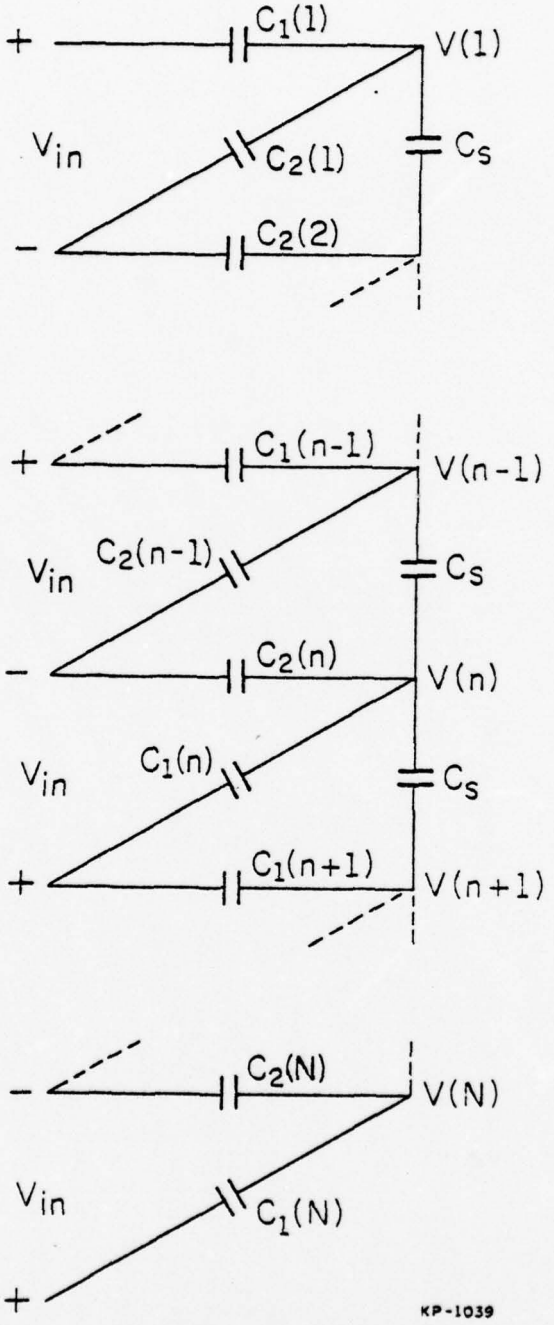

Figure 9. Circuit model for a semi-infinite CTWN transducer.

$$TW_i = \frac{Y_s(V_{i+1} - V_{i+2} + V_{i-1} - V_i) + V_o(Y_{1i} - Y_{i+1})}{Y_T + 2Y_s} \qquad (C\text{-}5)$$

$$= \frac{Y_s(TW_{i+1} + TW_{i-1}) + V_o(Y_{1i} - Y_{1i+1})}{2Y_s + Y_T}$$

Using the relation

$$Y_{1i} = Y_T - Y_{2i} \text{ and } Y_{1i+1} = Y_T - Y_{2i+1}$$

equation (C-5) is rewritten as

$$TW_i = \frac{Y_s(TW_{i+1} + TW_{i-1}) + V_o(Y_{2i+1} - Y_{2i})}{2Y_s + Y_T} \qquad (C\text{-}6)$$

Letting $V_o = 1$ and summing (C-5) and (C-6) yields

$$2TW_i = \frac{2Y_s/Y_T(TW_{i+1} + TW_{i-1}) + \left(\frac{Y_{1i}-Y_{2i}}{Y_T} - \frac{Y_{1i+1}-Y_{2i+1}}{Y_T}\right)}{1 + 2Y_s/Y_T} \qquad (C\text{-}7)$$

Define

$$\alpha_{wi} = \frac{C_{1i} - C_{2i}}{C_T}$$

then equation (-7) is rewritten as

$$\alpha_{wi} - \alpha_{wi+1} = 2TW_i(1 + 2Y_s/Y_T) - 2Y_s/Y_T(TW_{i+1} - TW_{i-1}) \qquad (C\text{-}8)$$

Equation (C-8) is broken into its real and imaginary parts by substituting

$$Y_s = G_a + j\omega C_s \text{ and } Y_T = j\omega C_T$$

which yields the real part

$$\alpha_{wi} - \alpha_{wi+1} = 2TW_i(1+2\alpha_R) - 2\alpha_R(TW_{i+1} - TW_{i-1}) \qquad (C\text{-}9)$$

and the imaginary part

$$0 = 2TW_i(2G_a/j\omega C_T) - (2G_a/j\omega C_T)(TW_{i+1} - TW_{i-1})$$

where $\alpha_R = C_s/C_T$.

The simultaneous solution of equations (C-9) yields

$$TW_i = \frac{\alpha_{wi} - \alpha_{wi+1}}{2} \qquad (C\text{-}10)$$

which is the result similar to the single tap analysis, however, the exact tap weight is now known in a multitap transducer environment. This is an important result since it allows the use of the impulse response model to accurately weight a CTWN transducer which simplifies design and analysis.

The above analysis applied to a semi-infinite tap array, however in reality transducers have finite lengths and the transducer periodicity abruptly ends. The tap weights for bandpass filters are normally approaching zero at the transducer ends and, therefore, perturbations caused by the end of the periodic structure are negligible for most filter applications. If transducer end effects are limiting filter performance, a procedure similar to Hartmann's [17] end effects analysis is performed and will compensate for the end taps.

D. Thin Film Loss Analysis

1). Single Tap Analysis

Figure 10 shows a single electrode in the capacitive weighted structure with the buss bars removed. Electrodes (1) and (3) define capacitor C_1 and conductance G_1 and electrodes (2) and (3) define

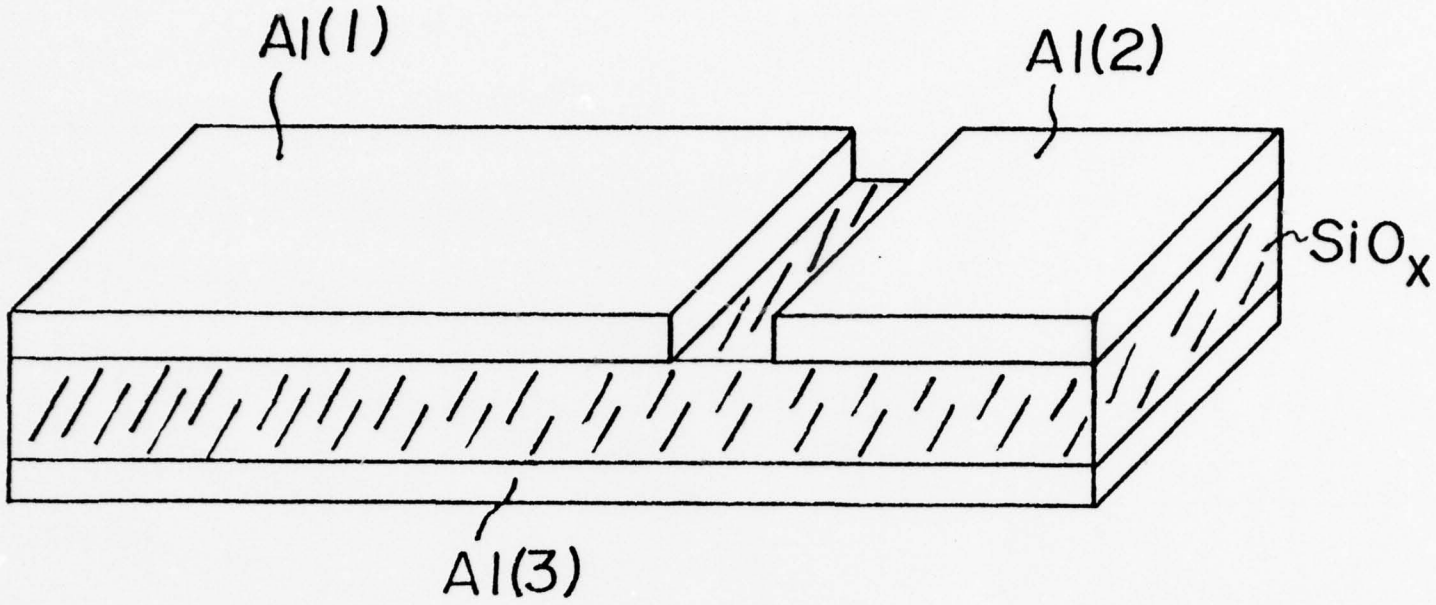

Figure 10. Physical structure of a single CTWN electrode.

capacitor C_2 and conductance G_2. The conductances G_1 and G_2 account for the metallic conductor resistance plus the capacitor dielectric conductance for C_1 and C_2 respectively. It is clear when the sum of the electrode areas (1) and (2) remains constant, irrespective of where the break in the electrodes occur, the following conditions hold:

$$\begin{aligned} &\text{i)} \quad C_1 + C_2 = C_T \\ &\text{ii)} \quad G_1 + G_2 = G_T \\ &\text{iii)} \quad G_1/C_1 = G_2/C_2 = \frac{G_1 + G_2}{C_1 + C_2} = G_T/C_T \end{aligned} \tag{D-1}$$

The equivalent circuit model used in the analysis is shown in Figure 11. The attenuator transfer function is

$$A = \frac{Y_1 - Y_2}{Y_1 + Y_2 + 2Y_S} \tag{D-2}$$

which expanded yields

$$\begin{aligned} |A| &= \sqrt{\frac{\omega^2 (C_1 - C_2)^2 + (G_1 - G_2)^2}{\omega^2 (C_1 + C_2 + 2C_s)^2 + (G_1 + G_2 + 2G_0)^2}} \\ \arg|A| &= \frac{\omega(C_1 - C_2)}{G_1 - G_2} - \frac{\omega(C_1 + C_2 + 2C_s)}{G_1 + G_2 + 2G_0} \end{aligned} \tag{D-3}$$

where G_0 represents the acoustic conductance for a single tap. Since all the capacitors and conductors are fabricated through identical processes, the thin film capacitor quality factor and substrate quality factor are equal for every tap, being defined as:

$$\begin{aligned} Q_T &= \frac{\omega C_1}{G_1} = \frac{\omega C_2}{G_2} = \frac{\omega C_T}{G_T} \\ Q_0 &= \omega C_s / G_0 \end{aligned} \tag{D-4}$$

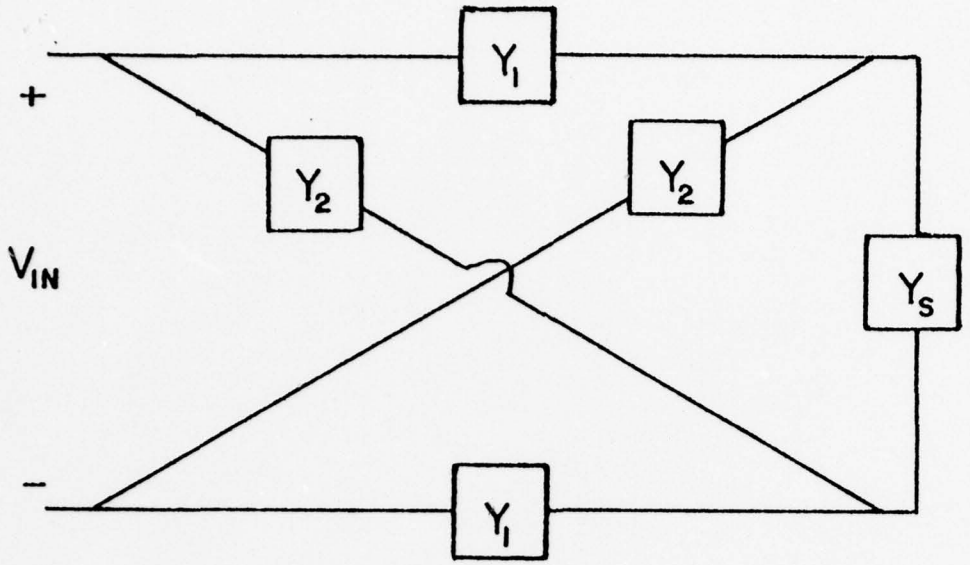

$$Y_1 = jwC_1 + G_1 \quad Y_2 = jwC_2 + G_2 \quad Y_s = jwC_s + G_s$$

Figure 11. Equivalent circuit model for a single finger pair including thin film losses.

Substitution of equations (D-1) and (D-4) into (D-3) with proper manipulation yields

$$|A| = \sqrt{\frac{\frac{(C_1-C_2)^2\ (1+Q_T^2)}{(C_1+C_2)^2\ Q_T^2}}{(1+2\alpha_R)^2 + (\frac{1}{Q_T} + \frac{2G_0}{\omega C_T})^2}}$$

$$\arg|A| = Q_T - \frac{1+2\alpha_R}{1/Q_T + 2G_0/\omega C_T} \qquad \text{(D-5)}$$

where $\alpha_R = C_s/C_T$. For high quality thin film capacitors, $Q_T \gg 10$, equation (D-5) is approximated as

$$|A| \approx K\,\alpha_w \text{ where } K \approx \frac{1}{1+2\alpha_R} \text{ and } \alpha_w = \frac{C_1-C_2}{C_1+C_2}$$

$$\arg|A| = Q_T\left(1 - \frac{(1+2\alpha_R)\ Q_0}{Q_0 + 2\alpha_R Q_T}\right) \quad \text{for } Q_{TF} > 10 \qquad \text{(D-6)}$$

which yields tap weight control without phase variations for constant Q_T and α_R, which is also the result obtained for the ideal lossless case.

The input admittance for the circuit of Figure 11 is

$$Y_{IN} = \frac{2Y_1Y_2 + Y_s(Y_1+Y_2)}{Y_1+Y_2+2Y_s} \qquad \text{(D-7)}$$

Upon expanding equation (D-7) using substitutions of equations (D-1) and (D-4) yields the total input admittance as

$$Y_{IN} = \frac{\omega C_s K^2}{Q_T}\left\{\frac{(1-\alpha_w^2)(1+4\alpha_R)}{2\alpha_R} + 2\alpha_R\right\} + \frac{\omega C_s K^2 \alpha_w^2}{Q_0}$$

$$+ j\omega C_s K^2\left\{\frac{(1-\alpha_w^2)(1+2\alpha_R)}{2\alpha_R} + 1 + 2\alpha_R\right\} \qquad \text{(D-8)}$$

where all Q^{-2} terms are assumed negligible. Using the definition $\alpha_R = C_s/C_T$ and substitutions of equation (D-4), the total input conductance and capacitance is

$$G_{IN} = \alpha_w^2 K^2 G_0 + K^2\{\frac{(1-\alpha_w^2)(1+4\alpha_R)}{2} + 2\alpha_R^2\}\ G_T = \alpha_w^2 K^2 G_0 + G_{TF} \qquad \text{(D-9)}$$

and

$$C_{IN} = (1 - \frac{\alpha_w^2}{(1+2\alpha_R)})\ \frac{C_s}{2\alpha_R} \qquad \text{(D-10)}$$

The total input conductance is the sum of two terms where $K^2\alpha_w^2 G_0$ is the acoustic conductance, as shown for the lossless case, and G_{TF} is the thin film metallic and dielectric conductance. The input capacitance, as shown in equation (D-10) is invariant to the thin film conductance for reasonably high Q's.

2). Thin Film Losses for Multi-Tap Transducer

The single tap analysis has shown that the voltage transfer ratio and input capacitance are unchanged for small dielectric losses but a measureable change occurs in the input conductance. For a given filter specification, substrate material and dielectric, the thin film loss will be calculated.

At center frequency, the acoustic conductance for an N tap transducer, as shown in Section II-B, is

$$G_a' = K^2 N_{eff}^2 G_0$$

where $N_{eff} = \sum_{n=1}^{N} \alpha_w(n) e^{j\omega T}$, G_0 is the acoustic conductance for a single tap and $\alpha_w(n)$ is determined by the thin film capacitors. The total thin film loss conductance is approximately

$$G_{TF} = K^2 N\{ \frac{(1-\overline{\alpha_w^2})(1+4\alpha_R)}{2} + 2\alpha_R^2 \} G_T \qquad \text{(D-11)}$$

where $\overline{\alpha_w^2}$ is the mean square tap weight value. The loss due to the thin film structure is calculated by

$$L_{TF} = \frac{1}{1 + \frac{G_{TF}}{G'_a}}$$

$$= [1 + \frac{N Q_0}{N_{eff}^2 Q_T}(\frac{(1-\overline{\alpha_w^2})(1+4\alpha_R)}{2\alpha_R} + 2\alpha_R)]^{-1} \qquad \text{(D-12)}$$

In order to minimize the loss, it is desirable to have a high thin film quality factor and a large mean square tap weight value. The filter specifications determine $\overline{\alpha_w^2}$, therefore, it is important to obtain the highest possible Q_T.

The designer has control on the choice of α_R and would like to minimize the thin film loss while still meeting any other fixed design criteria. The thin film loss approaches zero as G_{TF}/G'_a approaches zero and the minimum loss attainable as a function of α_R is found by taking the derivative of G_{TF}/G'_a with respect to α_R and setting the result to zero, which yields

$$\frac{\delta(G_{TF}/G'_a)}{\delta\alpha_R} = \frac{Q_0 N}{Q_T N_{eff}^2}[2 - \frac{2(1-\overline{\alpha_w^2})}{4\alpha_R^2}] = 0 \qquad \text{(D-13)}$$

Therefore, the minimum thin film loss as a function of α_R occurs when

$$\alpha_{R\,min} = \frac{\sqrt{1-\overline{\alpha_w^2}}}{2} \qquad \text{(D-14)}$$

This is the same condition found for the minimum Q_R' calculated in Section B. The thin film loss in equation (D-12) is further simplified to

$$L_{TF} \approx (1 + Q_R'/Q_T)^{-1} \qquad \text{(D-15)}$$

where $Q_R' = \frac{\omega C_o'}{G_a'}$. This is further verification of equation (D-14) since minimizing Q_R' for a given dielectric, Q_T, reduces the thin film losses. The total CTWN transducer Q including the thin film effects is

$$Q' = \frac{Q_R' \, Q_T}{Q_R' + Q_T} \qquad \text{(D-16)}$$

3). Experimental Determination of the Thin Film Parameters

All the CTWN transducers fabricated used an evaporated SiO_x dielectric layer and Al conductors for the electrodes. To determine the dielectric Q and the aluminum resistance, discrete thin film capacitors and resistors were fabricated as described in Appendix I. The capacitors consisted of an Al lower electrode, SiO_x dielectric and Al upper electrode with the capacitor area being .01 cm^2. The Al resistor is a meander pattern consisting of 324 squares taking into account the effects of the corners [21].

The Al deposited for the capacitor electrodes and the resistor pattern had a thickness ranging from 1900 to 2100 Å. This yielded a measured D.C. resistivity of approximately .15 Ω/square and this value is used in all the later calculations for the aluminum resistance.

The thin film capacitors were mounted on a header and lead bonded. The Al pads were kept short to cause negligible effects on the capacitor dielectric Q measurements. A General Radio twin tee bridge was used to obtain the capacitance and conductance measurements in the

frequency range from 30 MHz to 40 MHz, which is the highest measurement frequency range of the bridge. The capacitors were fairly uniform yielding Q's in the range from 30 to 40. The dielectric thickness ranged from 3000 Å to 8000 Å and capacitor yields were nearly 100% with dirt contamination being the cause for a few capacitor shorts.

III. EXPERIMENTAL RESULTS OF CTWN TRANSDUCERS FOR SAW BANDPASS FILTERS

The following sections describe the fabrication of CTWN transducers and present experimental data for a number of different CTWN transducers. The devices are designed to emphasize different aspects of the CTWN transducer filter capabilities and its limitations. The section discusses the theoretical designs, experimental results, design parameters and error analysis. The third harmonic response of the device is presented where applicable.

The frequency and time domain responses presented in the following sections are obtained through use of the Theoretical Effective Tap Amplitude Measurement (TETAM) system developed at CSL [22]. This allows for unique filter processing capabilities which minimize or eliminate the effects of RF coupling and many of the other spurious responses from the true SAW response.

A. Fabrication of CTWN Transducers

The devices presented in the following sections are all fabricated on 19 mil thick 128° $LiNbO_3$. This substrate material is used for its high acoustic coupling coefficient and low spurious bulk mode levels [23].

Al is deposited on the entire substrate to a thickness of 2000 Å $\pm$ 200 Å and a photo mask similar to that shown in Figure 12 is used to produce the lower finger electrodes using standard photolithographic techniques. The substrate is then placed in the vacuum system to deposit the SiO_x dielectric and Al upper layer using the procedure outlined in Appendix A. The SiO_x is evaporated over the entire substrate to the desired thickness and the Al layer is deposited to

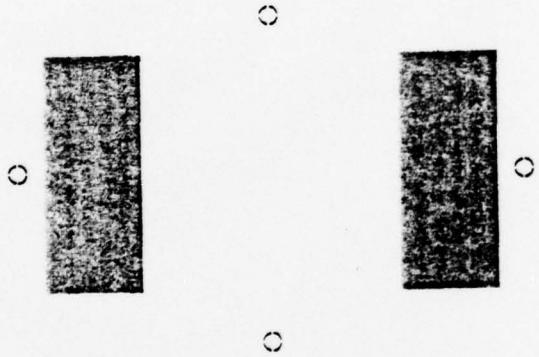

Figure 12. Typical mask for photolithographic production of the lower Al electrodes for a CTWN filter.

approximately 2000 Å onto the SiO_x without breaking vacuum. A mask similar to that shown in Figure 13 is used to fabricate the upper electrodes directly on top of the lower electrodes using standard photolithographic techniques which produced the capacitor structures. Through this fabrication procedure, hundreds of capacitors are made through a single photolithographic step and the relative capacitor values are extremely close since they are fabricated under identical conditions. The magnitude of each discrete capacitor is determined by the upper electrode area overlapping the lower electrode and the tap weight is very accurately determined by the difference of the lengths of the electrodes extending from opposite buss bars.

After photolithographic processing, the device back surface is lapped at approximately 3° and grooves, 5 mil wide by approximately 2 mil deep, are placed on the back through use of a wire saw. This back surface processing is necessary to scatter any bulk or plate modes that are generated and reduced the level, in most cases, greater than 60 db below the surface wave level.

The substrate is mounted on a header using silver conductive paint and lead bonded using a commercial thermo-compression lead bonder. After cooling, damping material is placed at the chip edges to absorb the SAW generated from the bidirectional transducers in the reverse direction. The material found to offer the best damping is AZ-1350J photoresist and is easily removed when necessary without leaving a residue. A finished device is pictured in Figure 14.

In order to measure C_T very accurately, a discrete thin film capacitor is fabricated directly on the SAW substrate. By direct

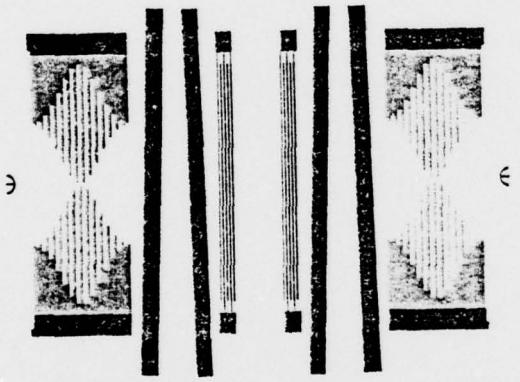

Figure 13. Typical mask for photolithographic production of the upper Al electrodes of a CTWN filter.

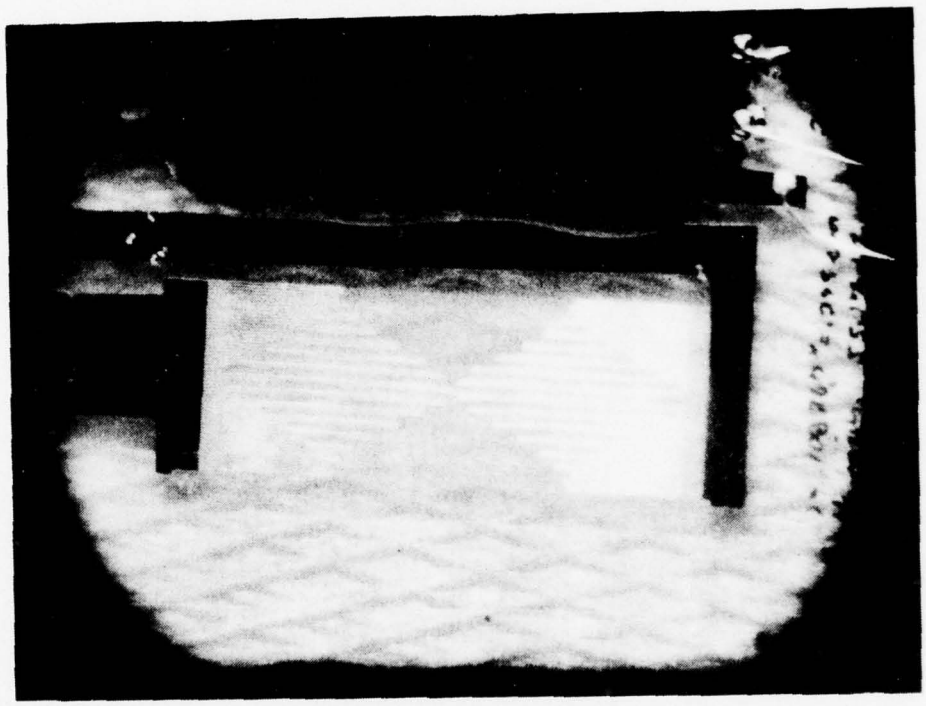

Figure 14. Photograph of a typical CTWN transducer after fabrication processing is complete. The cross-hatched lines are saw marks seen from the bottom surface which scatter bulk and plate modes.

measurement, the capacitance per unit area, $\overline{C_T}$, is found and used to evaluate C_T based on the device frequency and the upper electrode area given in wavelengths.

B. Tap Weight Verification

A 15 tap, double finger transducer having tap weights ranging from 0.015 to 1.0 with a center frequency of 51 MHz is used to evaluate the accuracy of capacity tap weighting. In this design, the sum of C_1 and C_2 are constant for every tap so that no tap phase errors occur. Overlap between positive and negative electrodes in the upper mask is prevented to eliminate any apodized interdigital transducer end effects due to fringing fields of the upper conductor pattern.

Two identical transducers are cascaded which yields a multiplication of the CTWN input and output transducer frequency responses

$$H_{input}(\omega) \cdot H_{out}(\omega) = H_{filter}(\omega)$$

and

$$H_{input}(\omega) = H_{out}(\omega)$$

which is equivalent to the convolution of the transducer time impulse responses. Theoretically, by using cascaded transducers the sidelobe rejection of the total filter is the square of the sidelobe rejection of the individual transducers and the level is directly related to the accuracy of the tap weights. If the tap weights of a single transducer are accurate to 1%, then the accuracy of the cascaded transducers is 0.01% which transforms to approximately 40 db greater sidelobe rejection. This is one of the big advantages of a CTWN filter over a normal apodized filter.

Figure 15 shows the theoretical and measured impulse response of the cascaded transducers which are in excellent agreement. The slight discrepancy between the theory and measured tap weights are due primarily to three sources: 1) diffraction, 2) tap weight round off errors in mask production, and 3) spurious bulk and plate mode generation. Figure 16a shows the superimposed theoretical and measured frequency responses. The passband shapes are in excellent agreement and the sidelobe rejection is 55 db.

By using the double finger transducer, MEL reflections are out of band causing no passband distortions and, theoretically, there is a strong third harmonic response [24]. Figure 16b is the third harmonic response of the cascaded filter showing good agreement with the fundamental response. Although double electrodes increase the photographic resolution requirements by 100% over a $2f_o$ sampled device, the third harmonic response of a CTWN transducer is very good and, when used, reduces the resolution requirements by 50% over a $2f_o$ sampled single electrode device. This is important when devices in the 1 GHz range are desired since the photographic resolution requirements limit higher frequency SAW fabrication.

Based on the CTWN model, the following pertinent theoretical and measured design data are provided in Table I for the CTWN transducer discussed in this section. The measured and calculated data are in good agreement verifying the CTWN impulse response model approach. The thin film Q_T for this device is rather low having a calculated value of approximately 24. This is due to the rather large beam width of 35 wavelengths which adds considerable Al resistivity of approximately 23 Ω per finger. The SiO_x dielectric Q is approximately 30, therefore,

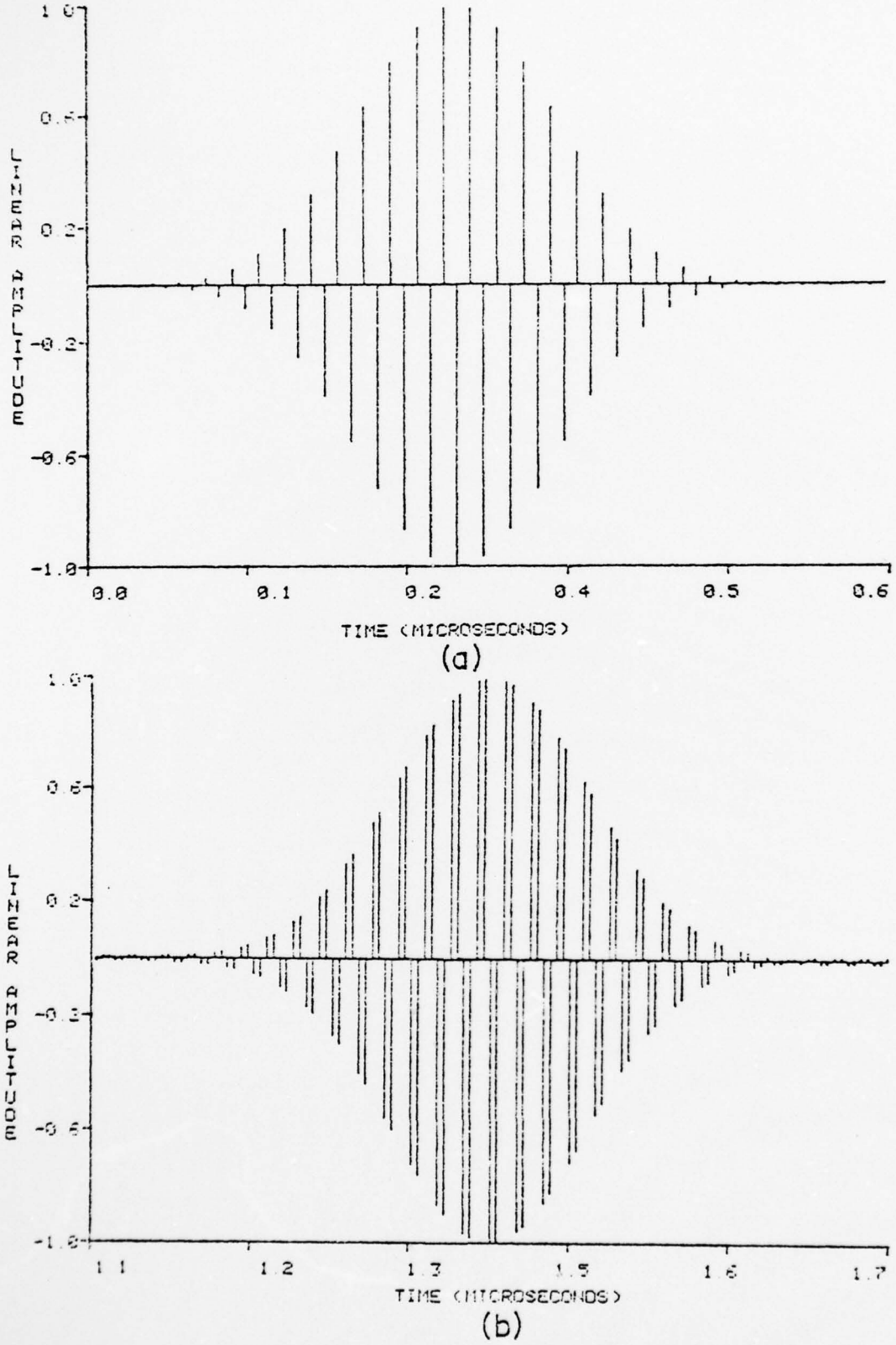

Figure 15. Impulse response of a 15 tap transducer a) theoretical and b) experimental.

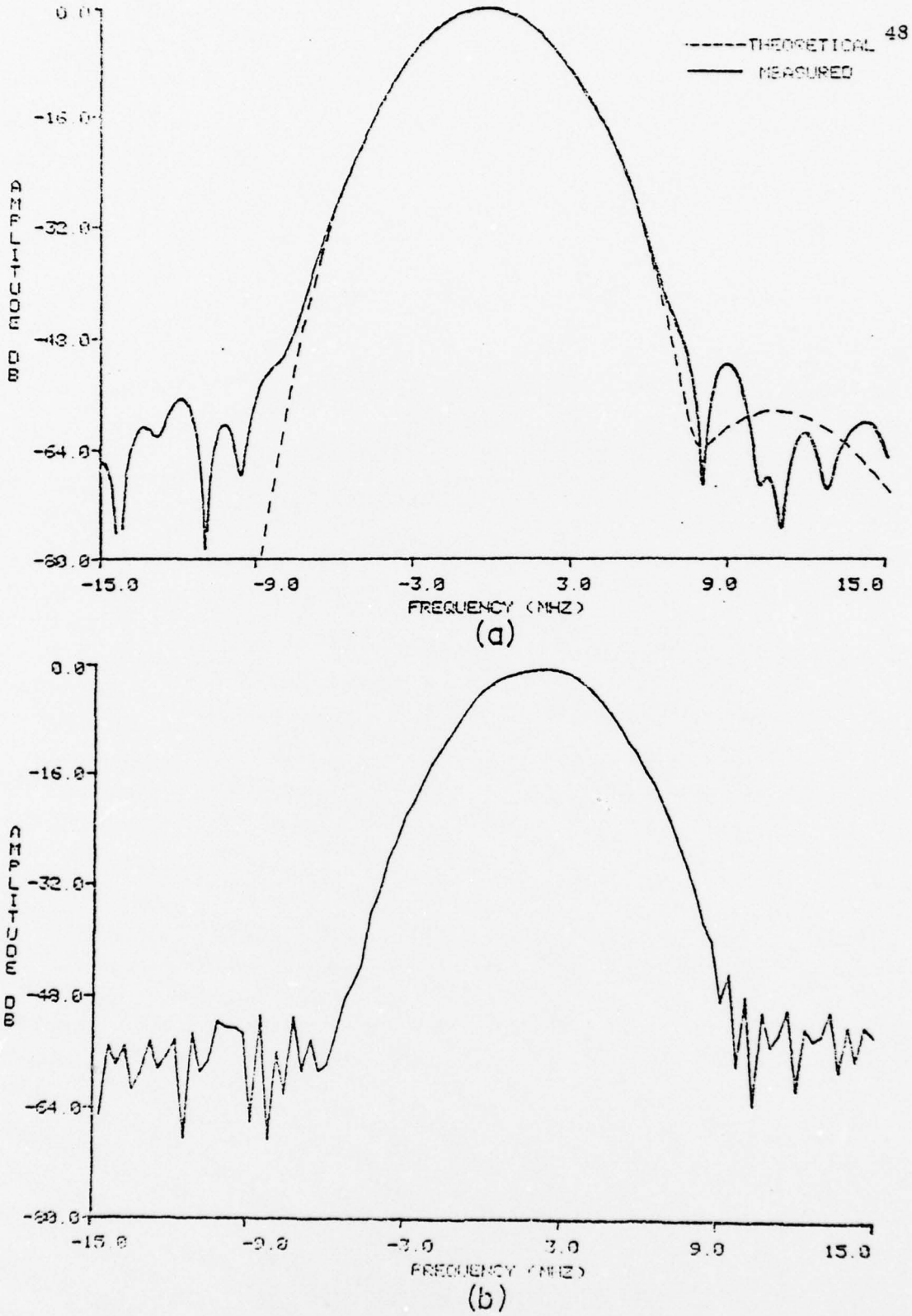

Figure 16. Frequency response of cascaded, 15 tap transducers. a) Theoretical and measured fundamental response and b) third harmonic.

TABLE I - Single Transducer

Design Parameters	Calculated	Measured
f_o (MHz)	50.6	50.6
BW(wavelength)	35.8	35.8
N (# of taps)	14.5	14.5
$\frac{N_{eff}}{\alpha_w^2}$	6.53	6.53
	0.33	0.33
$\overline{C_T}$ (pf/cm^2)	--	1.06×10^4
Q_T	18.2	--
C_s (pf)	1.83	--
C_T (pf)	2.96	--
α_R	0.62	--
C_o' (pf)	17.86	17.30
G_a' (μ mhos)	268.64	--
G_{TF} (μ mhos)	280.22	--
$G_a' + G_{TF}$ (μ mhos)	548.86	536.0
Thin Film Loss (db)	3.1	--
Unmatched IL (db) (Including thin film loss)	13.25	13.65

the Al resistivity greatly effects the overall thin film Q and is responsible for about one half of the total thin film loss. This encourages the use of narrow beam widths to minimize the thin film losses.

For the cascaded filter, the measured unmatched insertion loss is 35.2 db compared to the predicted value, based on the parameters of Table I, of 36 db. This is good agreement leaving only 0.8 db for bulk or other losses.

C. Bandpass Filter with Five Wavelength SAW Beam Width

The CTWN transducer uses the difference between two relatively large capacitors to determine the tap weight which is independent of the SAW beam width. The tap accuracy is limited only by the mask alignment and photolithographic resolution. Apodized transducers can not realistically achieve small beam widths due to diffraction and fringing fields at electrode ends, i.e., a 50 MHz apodized transducer having a tap weight of 0.01 and a beam width of five wavelengths requires a 4 μm overlap. This section evaluates a 63 tap, double finger transducer having a beam width of 5 wavelengths.

The theoretical tap weights and delay are shown in Figure 17 and include the tap delay modulation as discussed in Appendix B. The transducer has a center frequency of 51 MHz and a filter shape factor of 1.78. Figure 18a shows the frequency response of the cascaded filter. The passband shapes closely match except for a slight slope; however, the sidelobes are higher than predicted. The delay modulation is believed to be responsible for this level and the discrepancy between the measured and predicted sidelobe levels represents small measurement errors in the actual tap phases. The third harmonic response is shown in Figure 18b and there is good agreement with the fundamental.

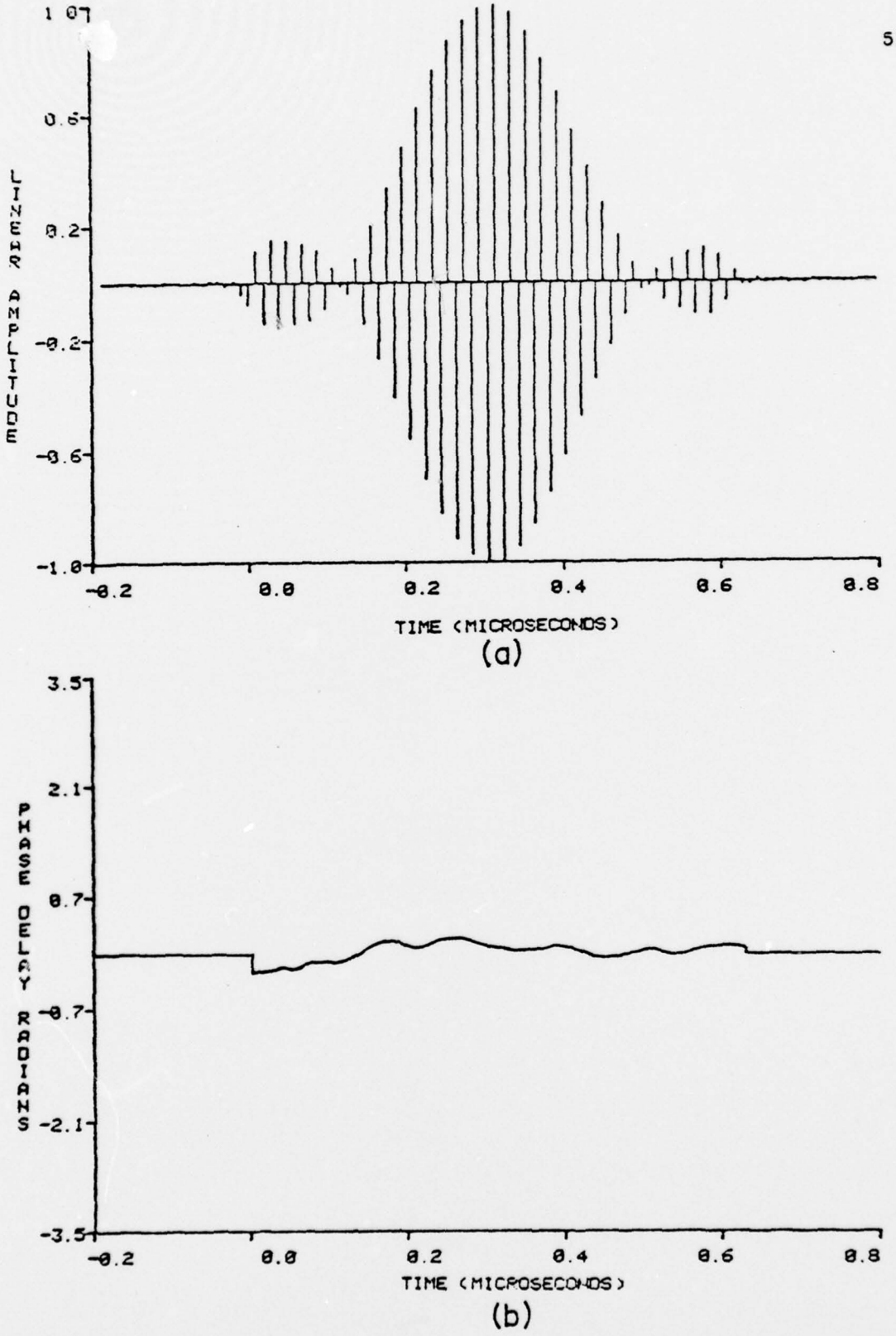

Figure 17. Transducer with 63 taps. a) Theoretical tap weights and b) the associated tap delay.

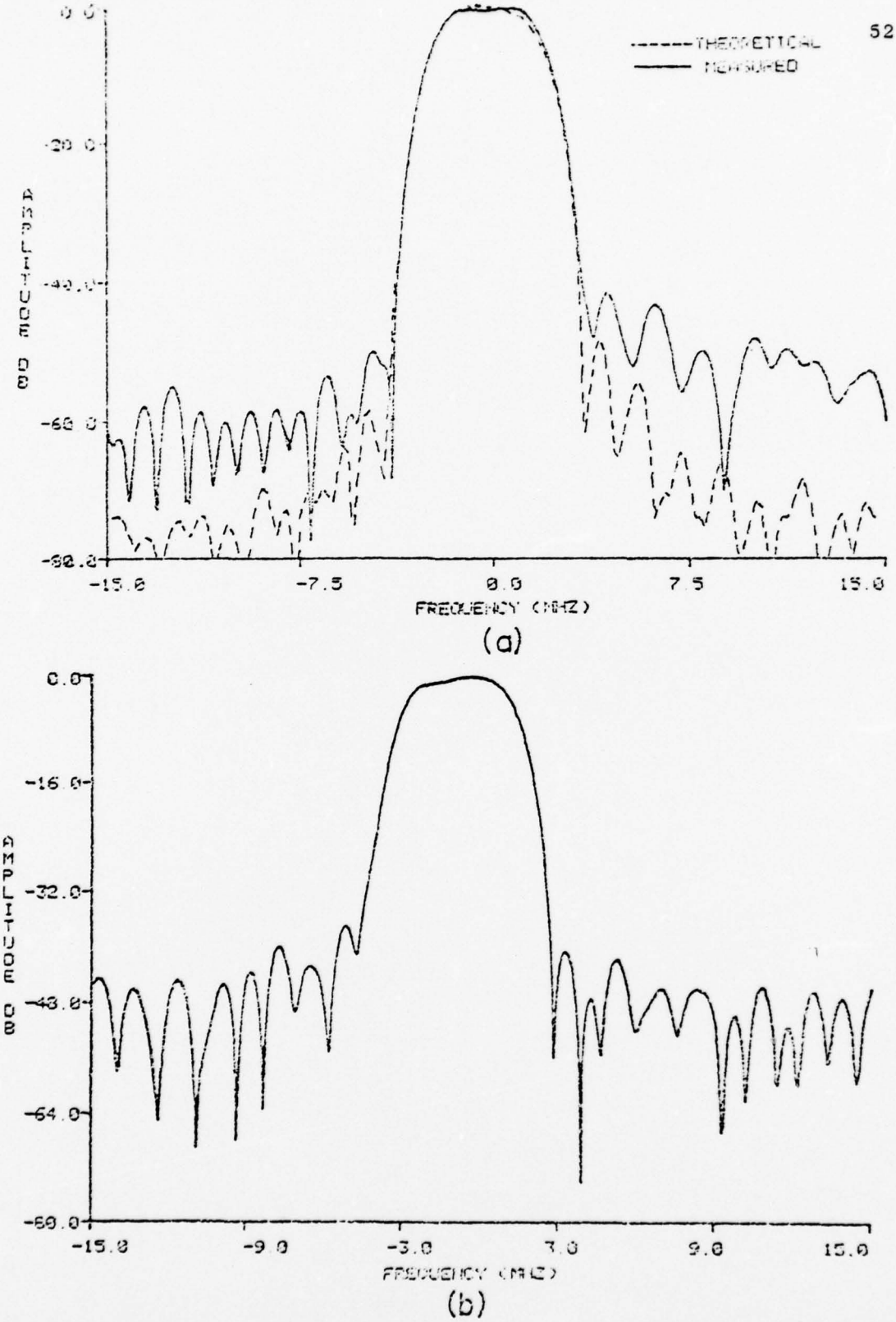

Figure 18. Frequency response of cascaded, 63 tap transducers.
a) Theoretical and measured fundamental response and
b) third harmonic.

The following pertinent theoretical and measured design data are provided in Table II for the CTWN transducer discussed in this section. The thin film loss of this transducer is reduced by 1 db over the 35 wavelength beam width transducer, discussed in Section III-B, due to the lower Al resistivity losses of the 5 wavelength beam width.

The measured unmatched insertion loss of the cascaded filter is 35.2 db and compares well with the predicted value of 36 db. The slight discrepancy could be accounted for in experimental measurement errors of the insertion loss or thin film Q_T. The experimental cascaded filter is pictured in Figure 19a.

D. CTWN Transducer Implementing Tap Deletion

The CTWN transducer has, in general, a higher Q than a similar apodized transducer which fundamentally leads to higher insertion loss for broadband high shape factor filters. It is desirable to eliminate small taps, which lower the transducer Q, while still producing highly selective filters. A theory for replacing a small number of taps with a single large tap with minimal frequency distortion has been developed.† The two conditions which make the replacement exact at center frequency, f_o, are

$$1) \quad \sum_{n=1}^{N} W_n e^{-j2\pi f_o t_n} = W_e e^{-j2\pi f_o \tau}$$

$$2) \quad \sum_{n=1}^{N} t_n W_n e^{-j2\pi f_o t_n} = \tau W e^{-j2\pi f_o \tau}$$

† "Tap Deletion Technique with Minimal Passband Distortion," S. Datta, B. Hunsinger, and D. Malocha, to be published.

TABLE II - Single Transducer

Design Parameters	Calculated	Measured
f_o (MHz)	51.0	51.0
BW(wavelength)	5.0	5.0
N (# of taps)	31.5	31.5
$\frac{N_{eff}}{\alpha_w^2}$	9.8 .22	9.8 .22
$\overline{C_T}$ (pf/cm^2)	--	12.18×10^3
Q_T	30	--
C_s (pf)	0.251	--
C_T (pf)	0.848	--
α_R	0.296	--
C_o' (pf)	11.10	13.20
G_a' (μ mhos)	167.39	--
G_{TF} (μ mhos)	109.38	--
$G_a' + G_{TF}$ (μ mhos)	276.77	268.37
Thin Film Loss (db)	2.18	--
Unmatched IL (db) (Including thin film loss)	15.00	14.60

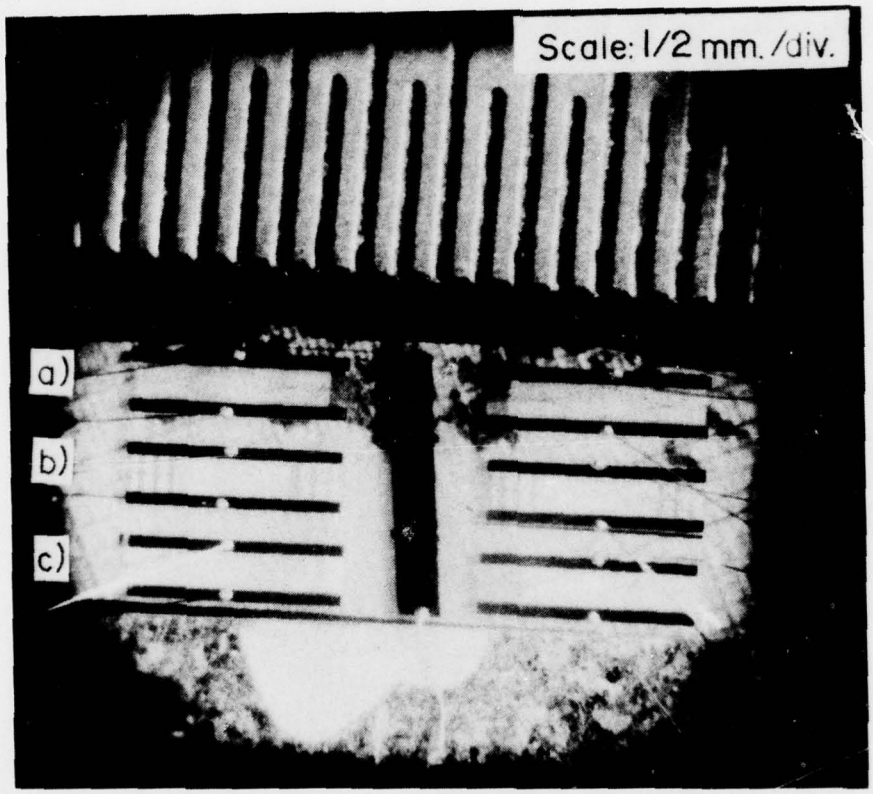

Figure 19. Three CTWN transducers with 5 wavelength beam widths and a center frequency of 51 MHz. A reference scale with 1/2 mm. per division is shown in the top half of the picture. a) Device of Section III-C, b) device of Section III-D and c) device of Section III-F.

where W_n is the n^{th} tap weight of the group of N taps to be deleted with delays t_n, W is the strength of a single tap to replace the group of N taps and τ is its delay. Condition 1) insures that the net strength is not altered at center frequency and condition 2) ensures that the phase slope at center frequency remains the same before and after tap replacement.

Figure 20 shows a conventional set of tap weights compared to a tap deleted set where a deletion of every fourth tap in the time sidelobes has occurred. The corresponding frequency responses are shown in Figure 21. The tap deletion introduces a slight passband ripple, lowers the sidelobes adjacent to the passband and raises the sidelobe level 15 MHz from the center frequency. This loss in sidelobe rejection approximately 15% away from center frequency is regained through the tuning of the transducer. By tuning, the passband ripple is reduced, the device insertion loss is minimized and the far band sidelobes are substantially reduced.

A double finger CTWN transducer using 58 taps, as shown in Figure 20b, and having a beam width of 5 wavelengths with a center frequency of 51 MHz is described. The delay modulation, described in Appendix B, and diffraction are applied to the tap weights to obtain the theoretically predicted results and compared to the measured response as shown in Figure 22a. There is excellent agreement between the predicted and measured frequency response indicating that tap deletion is controlled. The third harmonic is shown in Figure 22b and does not have as good a sidelobe selectivity. The probable cause is related to the tap delay modulation since the third harmonic is more sensitive to the tap positions. The time sidelobes are now composed of only 3 taps, with an average value of

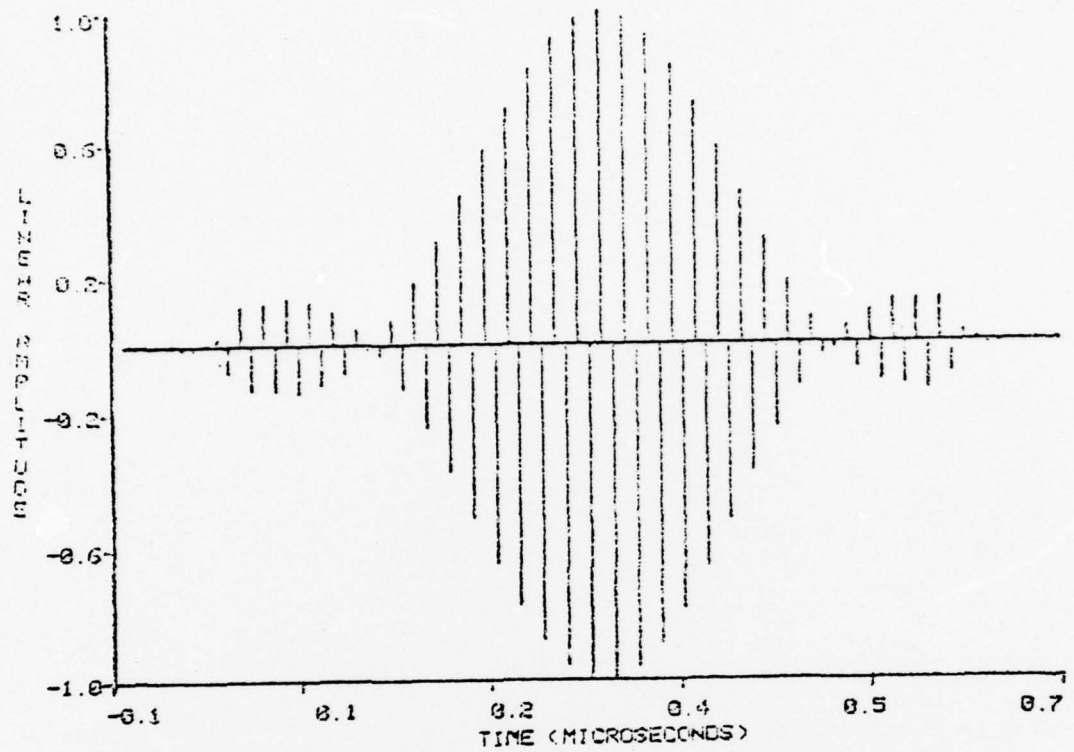

(a)

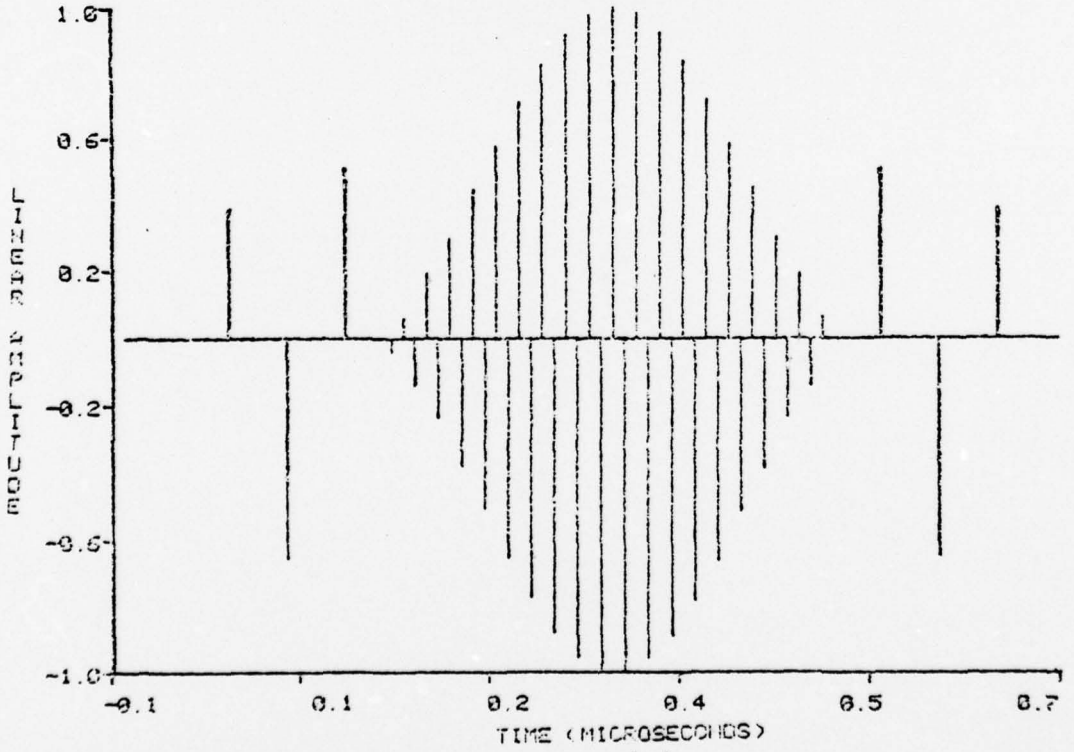

(b)

Figure 20. a) Conventional tap weights and b) tap deleted version with a 4:1 deletion in the time sidelobes.

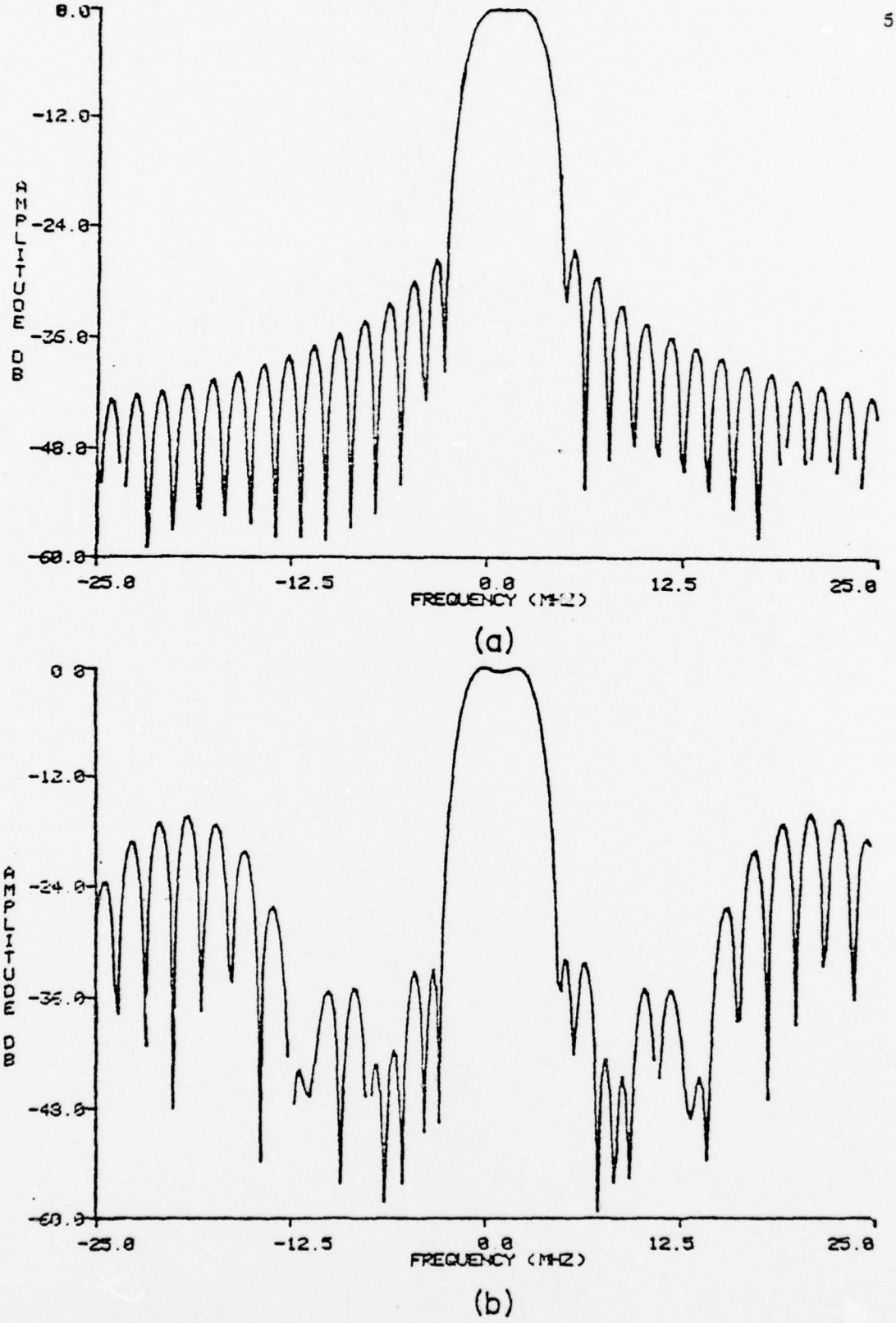

Figure 21. Frequency response of corresponding tap weights shown in Figure 20. a) Conventional tap weights and b) tap deletion.

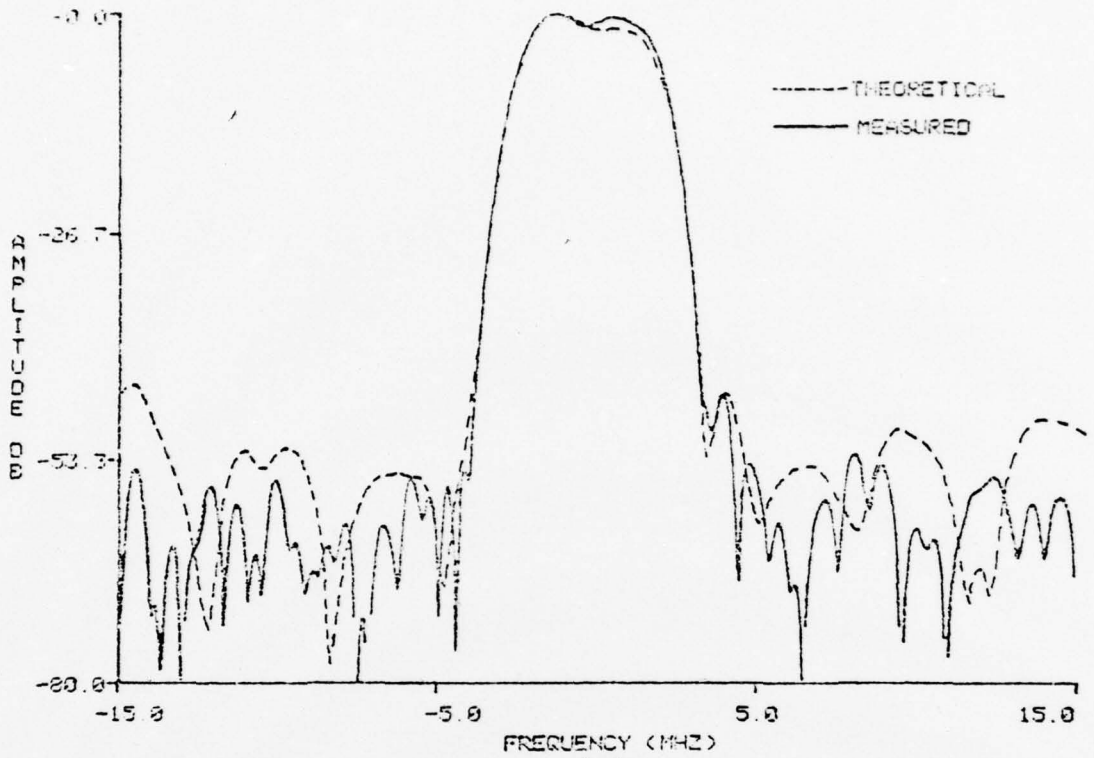

(a)

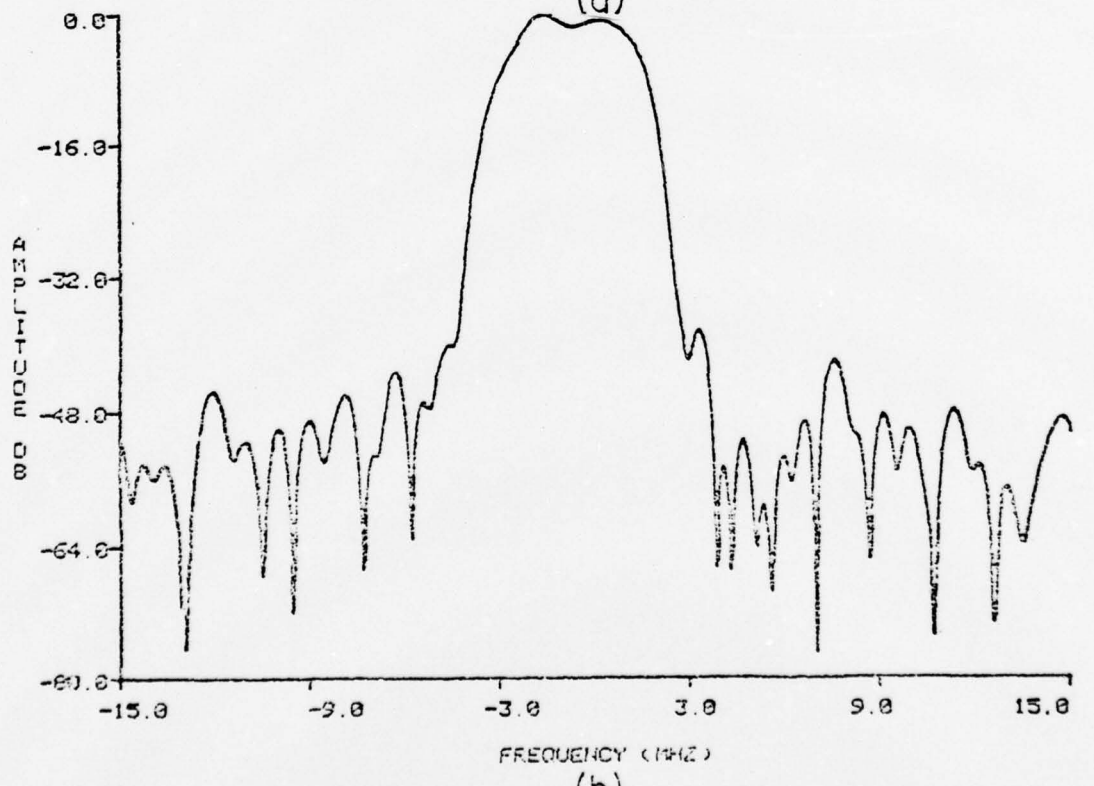

(b)

Figure 22. Frequency response of cascaded, tap deleted transducers.
a) Theoretical and measured fundamental responses and
b) third harmonic.

approximately 0.5, which enhances the effects of tap position errors on the frequency response.

Table III supplies the predicted and measured design data for the tap deleted device. The device described in this section corresponds to the tap deleted version of the device previously described in Section III-C. Both devices are fabricated under identical conditions and, therefore, a direct comparison of Table II and Table III parameters can be made. The acoustic conductance of the two devices does not significantly vary and does little to change the device Q. The input capacitance of the tap deleted transducer, with respect to the device of Section III-C, is reduced by approximately 15%, which is very close to the predicted value of 16.7% and verifies that a Q reduction is obtained through the use of tap deletion.

The cascaded filter measured insertion loss of 36 db agrees well with the predicted value of 35.4 db. The actual device is pictured in Figure 19b.

E. An Oversampled CTWN Transducer

Apodized transducers have not been widely used for producing oversampled devices since the weights of adjacent taps vary widely. Hunsinger and Kansy [25] developed a surface wave independent tap transducer (SWITT), however, it requires increased photolithographic resolution and two weighted transducers can not be directly cascaded. Since each finger strength of a CTWN transducer is independently controlled, rapidly varying tap weights can be implemented without increasing resolution requirements and the cascading of two transducers is possible.

TABLE III - Single Transducer

Design Parameters	Calculated	Measured
f_o (MHz)	51.0	51.0
BW(wavelength)	5.0	5.0
N (# of taps)	28	28
$\frac{N_{eff}}{\alpha_w^2}$	10.11	10.11
$\overline{C_T}$ (pf/cm^2)	0.35	0.35
Q_T	--	12.8×10^3
C_s (pf)	30	--
C_T (pf)	0.251	--
α_R	0.848	--
C_o' (pf)	0.296	--
G_a' (μ mhos)	9.25	11.4
G_{TF} (μ mhos)	178.22	--
$G_a' + G_{TF}$ (μ mhos)	88.49	--
Thin Film Loss (db)	266.7	240.21
Unmatched IL (db) (Including thin film loss)	1.75	--
	14.69	15.0

The majority of transducers fabricated use a uniform sampling rate of $f_s = 2f_o$, however, this limits the filter to only symmetrical passbands since the image response, which occurs at $(f_s - f_o)$, is superimposed on the direct response which is centered at f_o. Hunsinger and Kansy [25] introduced the concept of identifying each transducer element with a sample and then varying the sample rate to best meet the filter performance requirements. Using this concept, non-symmetrical filters are realized by choosing the sampling rate greater than twice the highest passband frequency so the image created by sampling is not superimposed on the direct passband response.

The Fourier transform of a general bandpass filter at baseband results in inphase ($h_i(t)$) and quadrature ($h_q(t)$) time samples. The impulse response is written as

$$h(t) = h_i(t) \cos \omega_o t + h_q(t) \sin \omega_o t$$

or

$$h(t) = a(t) \cos \phi(t)$$

where

$$a(t) = 2(h_i(t)^2 + h_q(t)^2)^{1/2}$$

and

$$\phi(t) = \omega_o(t) + \tan^{-1}\left(\frac{h_q(t)}{h_i(t)}\right) .$$

For a sampling rate of $f_s = 2f_o$, $\omega_o t = n\pi$ which yields

$$h(t) = h_i(t)$$

and there is only the inphase component. For symmetrical filters $h_q(t) = 0$ and there is no distortion, however, for asymmetric filters $h_q(t) \neq 0$ and a $2f_o$ sampling rate can not be used. For an arbitrary sampling rate, greater than $2f_o$ such that the image is not superimposed on the direct response, the samples occur at a uniform spacing but do not fall on the

peaks of the time envelope, as shown in Figure 23. The special case of $f_s = 4f_o$, $\omega_o t = n\pi/2$, yields independent inphase and quadrature components and is discussed in Section F.

The theoretical sampled impulse response used for the CTWN transducer is shown in Figure 24. The sampling rate is chosen arbitrarily as $f_s = 2.56\ f_o$ and results in rapidly varying tap weights. The device center frequency is $f_o = 64.24$ MHz with a sampling rate of 164.45 MHz which centers the image response at 100.21 MHz. The transducer has a 55 wavelength beam width with respect to the center frequency, a shape factor of 1.59 and contains 30 taps. The superimposed theoretical and measured frequency responses of the cascaded filter are shown in Figure 25. The direct and image responses have the correct passband shape and occur at the proper frequencies in relation to the sampling rate. The direct response has a slight passband ripple while the image has a sizeable ripple compared to the theoretical and the device sidelobe level is limited to approximately 32 db. The sidelobe level is limited for the following reasons: 1) the steep skirts and high selectivity require many small taps which raises the bulk to SAW distortion level, 2) the impulse response contains two time sidelobes and small tap phase errors are enhanced, and 3) due to oversampling, the filter performance is very sensitive to any tap weight or phase errors. The increased ripple in the image passband with respect to the direct is primarily due to the interaction of the SAW image response with the bulk waves from the direct response. The image response is at a higher level than the direct response due to better impedance matching of the load.

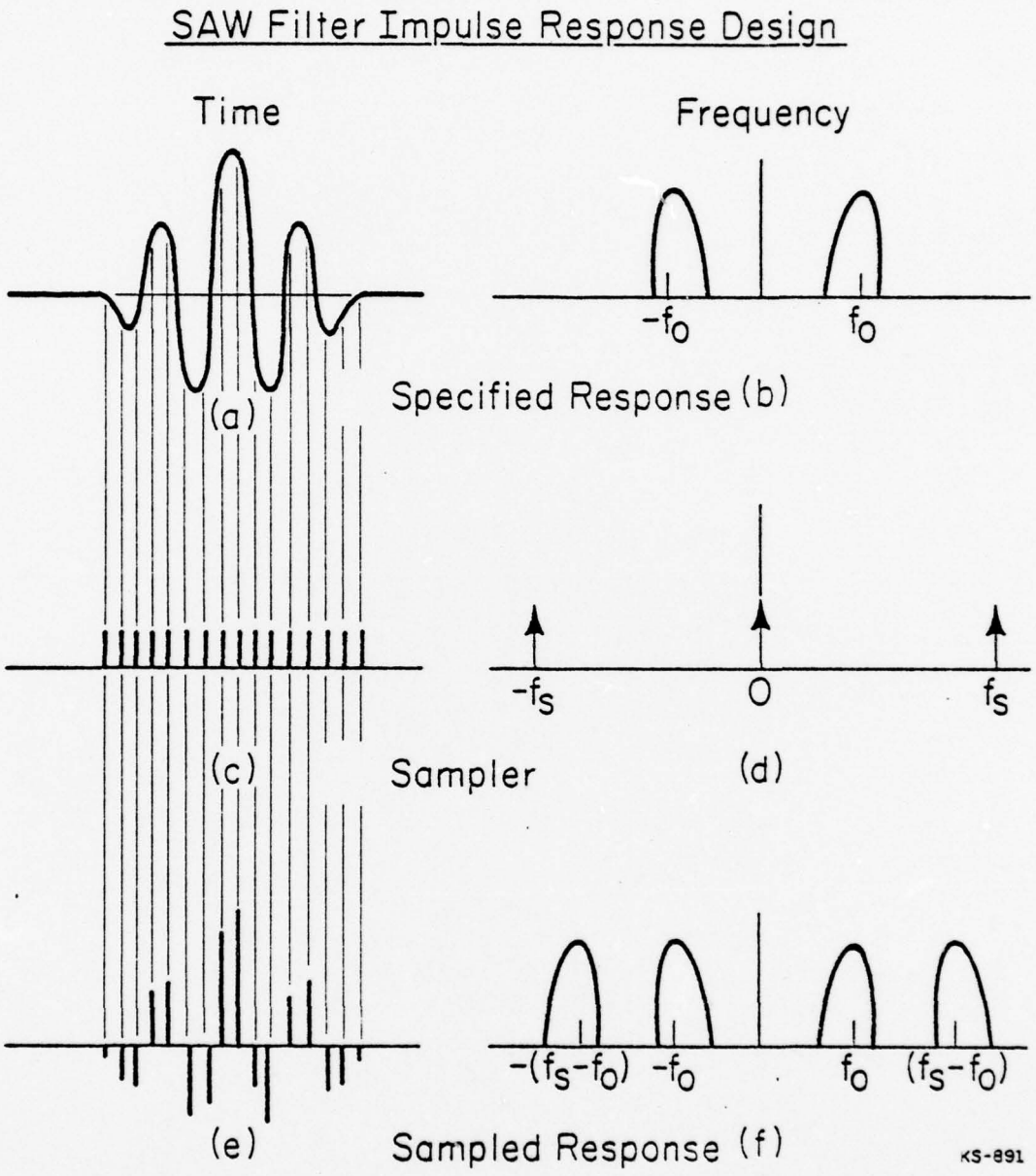

Figure 23. Oversampling technique. a) Specified time response. b) Specified frequency response. c) Time sampler. d) Frequency sampler. e) Result of multiplication of the specified time response and the time sampler. f) Result of convolution of the specified frequency response and the frequency sampler.

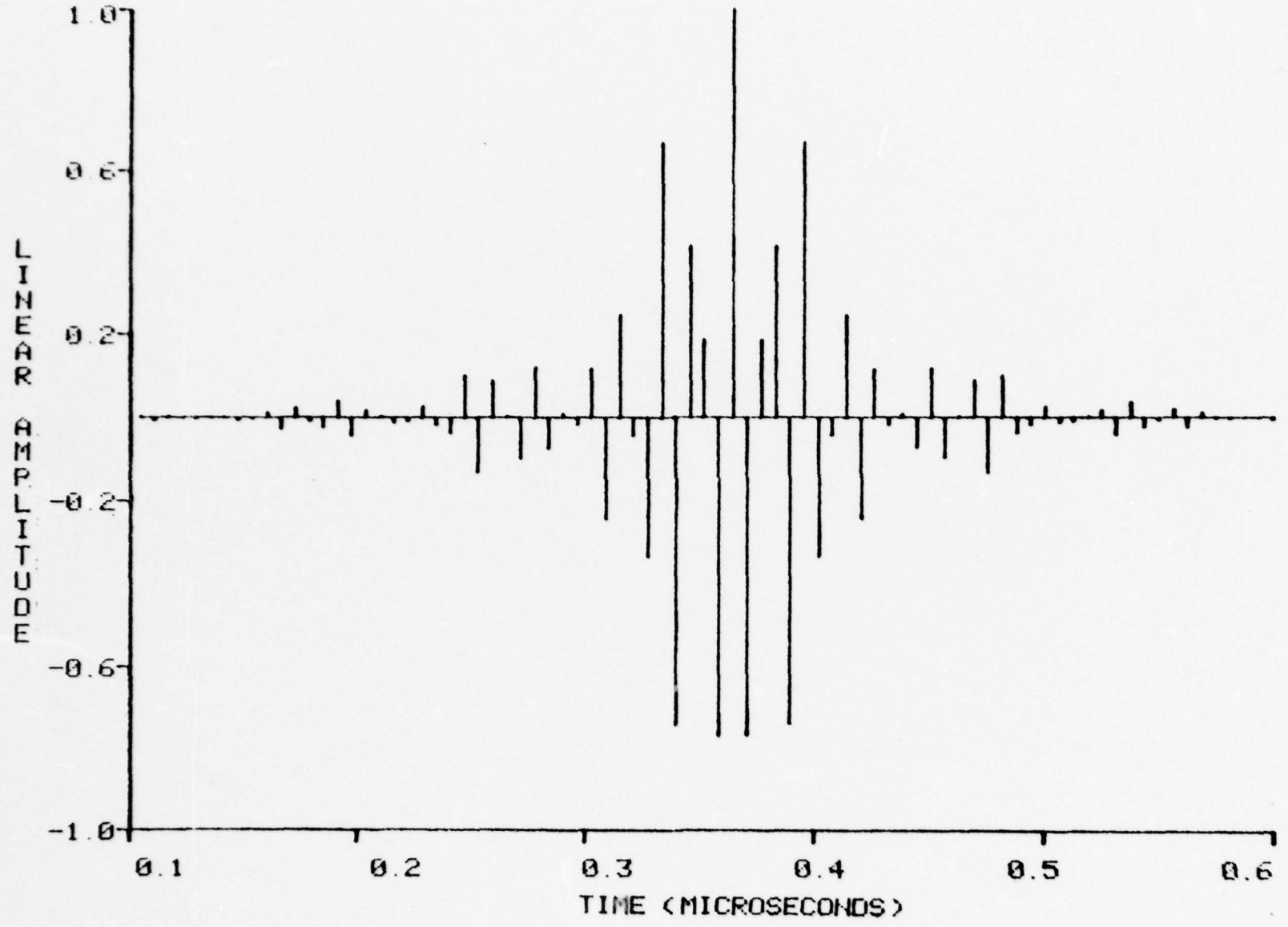

Figure 24. Theoretical time sampled impulse response with $f_s = 2.56\ f_o$.

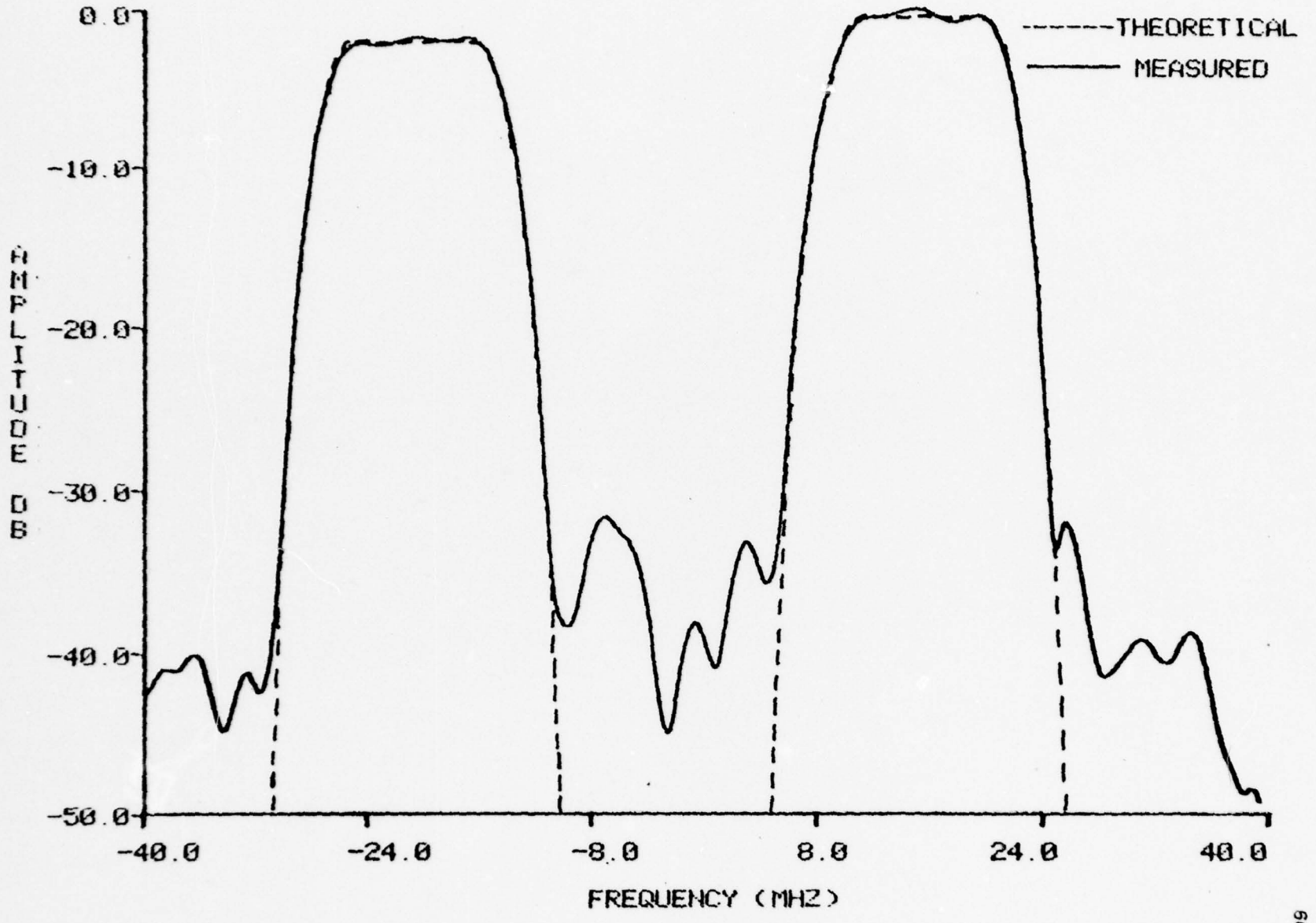

Figure 25. Theoretical and measured direct and image responses of cascaded, oversampled transducers with $f_s = 2.56\ f_o$.

Table IV provides the pertinent calculated and measured design parameters for the oversampled device. The thin film insertion loss of this transducer is approaching 11 db which is extremely large. This is anticipated for two reasons: 1) the beam width is relatively wide yielding a calculated Al resistance of 61 Ω which accounts for a substantial part of the loss and 2) because the device is broadband and highly selective the effective number of taps is extremely small in comparison to the total number of taps which fundamentally leads to high loss for the CTWN transducer. The measured total conductance of the device is substantially higher than predicted which indicates the thin film conductance is greater than calculated.

F. Inphase-Quadrature Sampled CTWN Transducer

Section E introduced the concept of oversampling and this section describes the special case of inphase-quadrature sampling ($f_s = 4f_o$). For filters with symmetrical passband responses, each pair of fingers has the same tap weight and produces symmetrical passbands centered at f_o and $3f_o$ which corresponds to the double finger transducer [24], as confirmed in the experimental devices of Section III-B, C, D. However, when an asymmetric passband is required, each finger assumes a unique tap weight which produces the desired response centered at f_o and $3f_o$ with the image response being the inverse of the direct response.

Each finger of a CTWN transducer corresponds to one time sample; with the even taps corresponding to the inphase samples and the odd taps corresponding to the quadrature samples. The theoretical taps

TABLE IV - Single Transducer

Design Parameters	Calculated	Measured
f_o (MHz)	64.24	64.24
f_s (MHz)	164.45	164.45
N (# of taps)	30	30
$\frac{N_{eff}}{\alpha_w^2}$	3.7	3.7
$\overline{C_T}$ (pf/cm^2)	0.10	0.10
Q_{TF}	9.47×10^3	--
C_s (pf)	14	--
C_T (pf)	1.251	--
α_R	1.555	--
C_o' (pf)	0.809	--
G_a' (μ mhos)	22.1	24.2
G_{TF} (μ mhos)	54.4	--
$G_a' + G_{TF}$ (μ mhos)	621.47	--
Thin Film Loss (db)	675.87	934.63
Unmatched IL (db) (Including thin film loss)	10.94	--
	20.66	21.0

are shown in Figure 26. The samples in the main timelobe correspond directly to the fingers of the CTWN transducer while the samples in the time sidelobes correspond to a pair of fingers. The CTWN transducer consists of 35 taps with a center frequency of 51 MHz and a 5 wavelength SAW beam width. The superimposed theoretical and measured frequency responses of the cascaded filter is shown in Figure 27a. The predicted and measured responses agree well except at the high passband side which is probably due to tap weight and delay errors occurring during fabrication processing. The image response, shown in Figure 27b, is a near perfect reflection of the direct response and occurs at 3 times the center frequency. This indicates that with proper design, the image response could be used with a resulting decrease in photographic resolution of 2/3.

Table V provides the pertinent calculated and measured design parameters for the inphase-quadrature weighted device discussed in this section. There is good agreement between the predicted and measured data with a slight difference in the input capacitance. The thin film insertion loss is rather substantial at a level of 3 db per transducer. It would be feasible to lower the thin film loss and transducer Q by using the tap deletion technique previously described.

The cascaded filter unmatched insertion loss of 34.42 db is lower than the calculated value of 38.36 db. The actual device is pictured in Figure 19c.

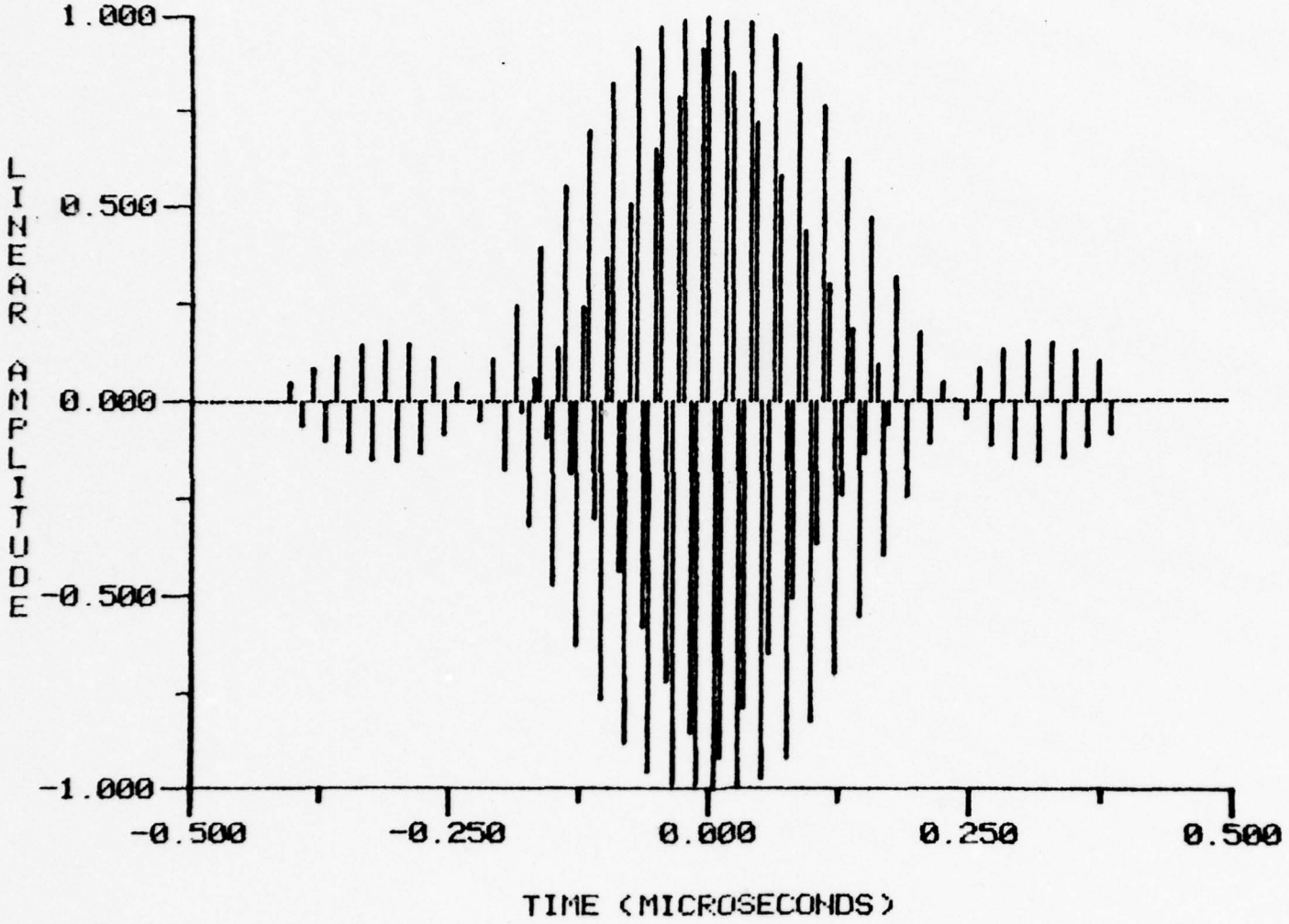

Figure 26. Inphase-quadrature sampled impulse response.

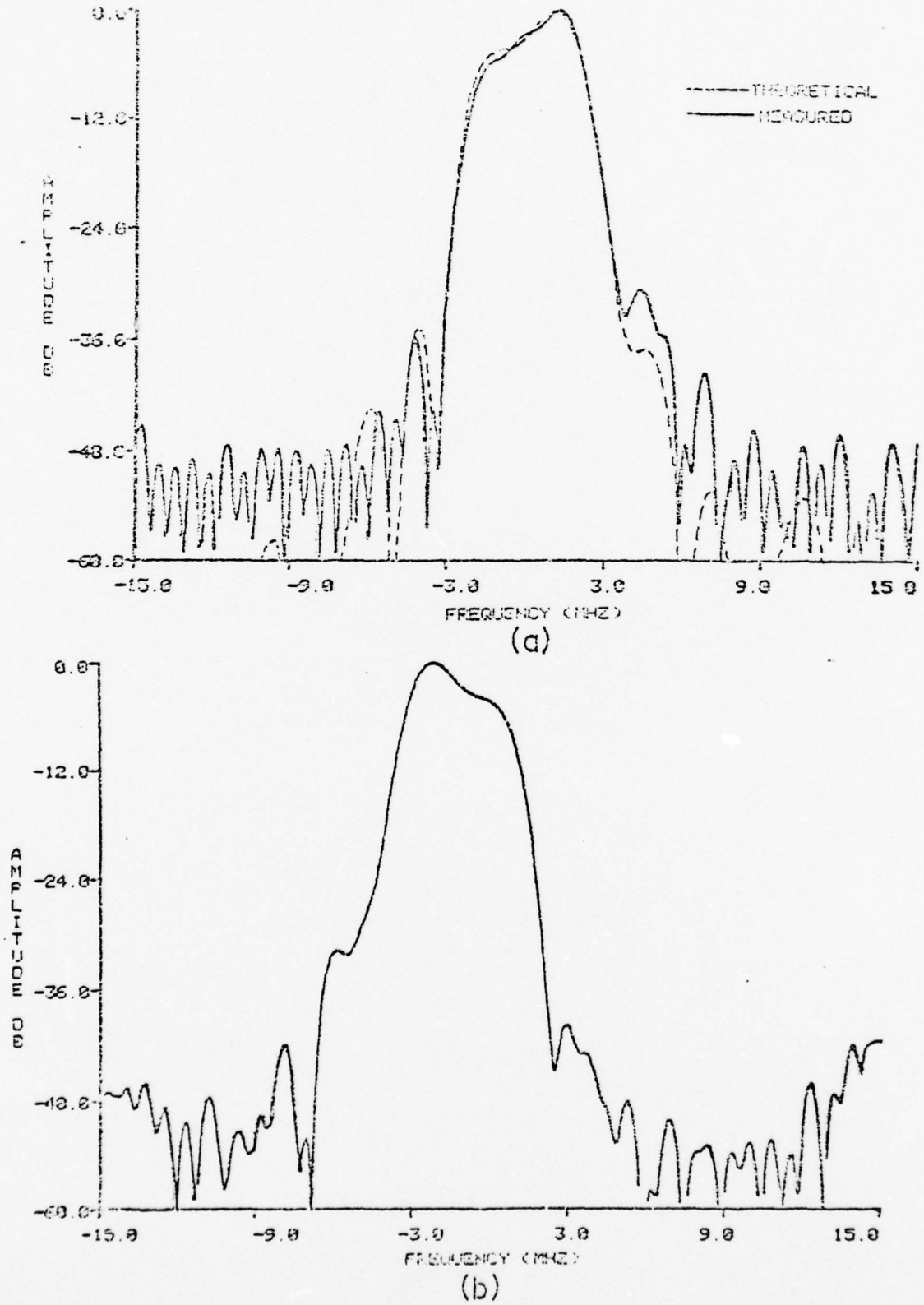

Figure 27. Frequency response of inphase-quadrature, cascaded transducers. a) Theoretical and measured fundamental response and b) third harmonic.

TABLE V - Single Transducer

Design Parameters	Calculated	Measured
f_o (MHz)	51.0	51.0
BW(wavelength)	5.0	5.0
N (# of taps)	35	35
$\frac{N_{eff}}{\alpha_w^2}$	8.6	8.6
	0.217	0.217
$\overline{C_T}$ (pf/cm^2)	--	12.18×10^3
Q_T	30	--
C_s (pf)	0.251	--
C_T (pf)	0.848	--
α_R	0.296	--
C_o' (pf)	12.62	15.4
G_a' (μ mhos)	128.7	--
G_{TF} (μ mhos)	128.77	--
$G_a' + G_{TF}$ (μ mhos)	257.47	255.70
Thin Film Loss (db)	3.01	--
Unmatched IL (db) (Including thin film loss)	16.18	14.21

G. Discussion and Comments

The experimental devices described in the previous sections verify the CTWN model and show the great versatility of the structure. The devices presented are a representative cross section of typical and varying designs and are not all inclusive.

The limiting performance factor of the devices presented is the uncontrolled modulation of the tap positions. In order to obtain distortion free passbands and high sidelobe selectivity the tap positions must be accurately set. Lower finger patterns commercially produced by high controlled laser exposure and accurate step and repeat procedures will minimize these errors.

The dielectric material used was evaporated SiO_x. The films produced were of consistent quality, could be easily grown and adhered well to the substrates. However, a dielectric having a higher Q is very desirable to further reduce the thin film losses. It is anticipated that Q's of 100 or better can be achieved for thin film capacitors in this type of structure [26].

Surface wave beam widths of five wavelengths have been presented with excellent results. This leads to the possibility of even smaller beam widths of possibly one wavelength which has applications in SAW waveguides or other structures desiring a weighted time response and a narrow uniform beam width.

Cascaded transducers have been presented which yield good filter performance. All the devices presented used two identical transducers in cascade, however, transducers having different sampling rates or center frequencies can be cascaded. In this manner, non-symmetrical filter responses can be realized by using two symmetrical passbands having

different frequencies. Similarly, two different sampled transducers used in cascade can produce decreased distortions due to second order effects, such as MEL reflections and bulk waves, or produce an asymmetric filter response.

Tap deletion was used to reduce the CTWN transducer Q and yielded encouraging results. Other techniques also need to be explored to further reduce the CTWN transducer Q and thereby lower the insertion loss of broadband, high selectivity filters.

IV. CONCLUSION

A weighted transducer structure for generation of a uniform beam surface acoustic wave has been developed. Thin film capacitors in a bridge type network are used to adjust the voltage on each tap to control the magnitude and phase of the generated SAW while maintaining uniform length electrodes. Experiments have been conducted on a number of CTWN transducers with various designs and yielded consistently good agreement between the predicted and measured data.

The thin film losses for a general CTWN transducer has been analyzed based on the thin film and substrate material parameters. The thin film structure introduces an additional loss mechanism which raises the device insertion loss but does not degrade the filter frequency selectivity. Thin film dielectric materials compatable with the CTWN transducer structure and having a high Q in the VHF and UHF frequency range will minimize filter insertion loss.

A model which accurately describes the multitap CTWN transducer input admittance, insertion loss, and electrical Q has been devised. Design procedures for capacitive weighted bandpass filters has been developed and verified.

The experimental filters presented demonstrated the following features:

1) devices are easily fabricated with consistent results,

2) tap weights are accurately controlled and have a wide dynamic range,

3) small beam widths with accurate tap weight control on a reduced substrate size are practical,

4) input and output transducers are both weighted to achieve more versatile design,

5) higher harmonics are good reproductions of the fundamental response making harmonic operated filters more practical and a reduction in fabrication resolution is obtained.

6) oversampled devices are easily fabricated using the CTWN transducer, and

7) tap deletion is used to reduce the transducer Q for broadband, highly selective filters.

APPENDIX A

Device Fabrication

The devices were fabricated in a commercial CHA vacuum system using an oil diffusion pump with the base pressure of the system maintained below 2×10^{-6} Torr before any evaporations proceeded. The substrates were mounted on a heating block in the vacuum system and allowed to bake 1 hr at approximately 200°C before depositing the films and maintained at this temperature during evaporation. The SiO_x was evaporated from a Drumheller source and a tungsten helix coil was used for the Al evaporation. The source to substrate distance was 27 cm which yields very uniform films over the area of interest (less than 5 cm^2) [21]. A shutter is placed between the source and substrate to quickly block the vapor stream when the desired film thickness is obtained.

Before the SiO_x was evaporated, a period of 10 minutes was allowed for the Drumheller source to heat to a uniform temperature. During this time, the system background pressure was raised to 5×10^{-5} Torr by leaking in bottled O_2. This was done to control the background O_2 pressure to a known level so any oxidation process of the evaporated material would be constant, yielding films of uniform composition from run to run. After the 10 min period, the shutter was opened and the deposition occurred at a rate of approximately 7 Å/sec until the desired film thickness was obtained.

A quartz crystal monitor was placed at approximately the same height and in close proximity to the substrate in order to monitor the film growth. The crystal is calibrated in units of frequency change

per angstrom of film thickness for a given deposited material [21]. The absolute film thickness is determined after deposition using interferometry techniques and the crystal calibration is obtained after a few standard runs. The film thickness was consistently predicted within 7% by use of the quartz crystal readings.

APPENDIX B

TAP POSITION ERROR ANALYSIS

An error analysis is conducted to determine the distortion effects of tap position modulation on filter performance. The areas of investigation presented are: 1) the experimental measurement of the errors, 2) the distortion effects on the specified response based on these errors, and 3) the experimental verification of the predicted error response with a measured transducer. The devices described in Section III-C, D, and F were all built using the same master art for the lower fingers and the following error analysis is applicable to all three.

1) Experimental Measurement of Errors

The photographically reduced master art is used to expose the photoresist on an aluminized substrate which is etched; leaving the lower electrodes. A profilometer is used to obtain the center to center tap distances by dragging a micro-stylus over the substrate. The electrode Al edge represents a discontinuity which the profilometer detects and converts to a DC signal and is recorded. In this manner both the edge position and Al thickness is recorded on a strip chart and the nearly uniform step height and width distinguishes the electrodes from random discontinuities. The profilometer represents a point sampler and any variation of the electrodes perpendicular to the probe velocity is neglected. Effects of modulation in the finger lengths is small since any sinusoidal variation is canclled when the transducer integrates across the beam.

The tap positions with respect to a reference point is carefully measured from the strip chart recorder and converted to tap delays. The data were processed to remove measurement errors and inconsistencies which

yielded the most representative tap error positions. The data were read into a computer file for analysis.

2) Distortion Effects on the Specified Response Based on the Measured Error

Figure 28 is the tap amplitude and delay response for a 60 electrode transducer having alternating tap weights of +1 and -1. Figure 29 is the response for the same transducer but with the measured tap delay included. The peak phase ripple is never greater than .2 radians which represents a phase distortion of approximately 3%. Figure 30a shows the sin x/x frequency response expected for 60 electrode transducer. Figure 30b shows the non-symmetric frequency response with increased sidelobe level of the 60 electrode transducer with tap delay modulation. The difference between the two responses is the error due to delay modulation, shown in Figure 31, and has its maximum at the high side of the passband and decreases on either side.

The convolution of the error response with the specified response yields the predicted response with the distortion effects due to tap delay errors. The specified tap amplitude and phase response is shown in Figure 32, with the transformed frequency response in Figure 33a. The multiplication of the time responses of Figures 32 and 28 is equivalent to convolving the frequency responses of Figures 30a and 33 and yields the specified frequency and time responses without perturbation, as expected. However, the multiplication of the time responses of Figures 32 and 29, which is equivalent to convolving the frequency responses of Figures 30b and 33, yields the desired tap weights but now has tap delay modulation and the specified frequency response has been distorted as shown in Figure 33b.

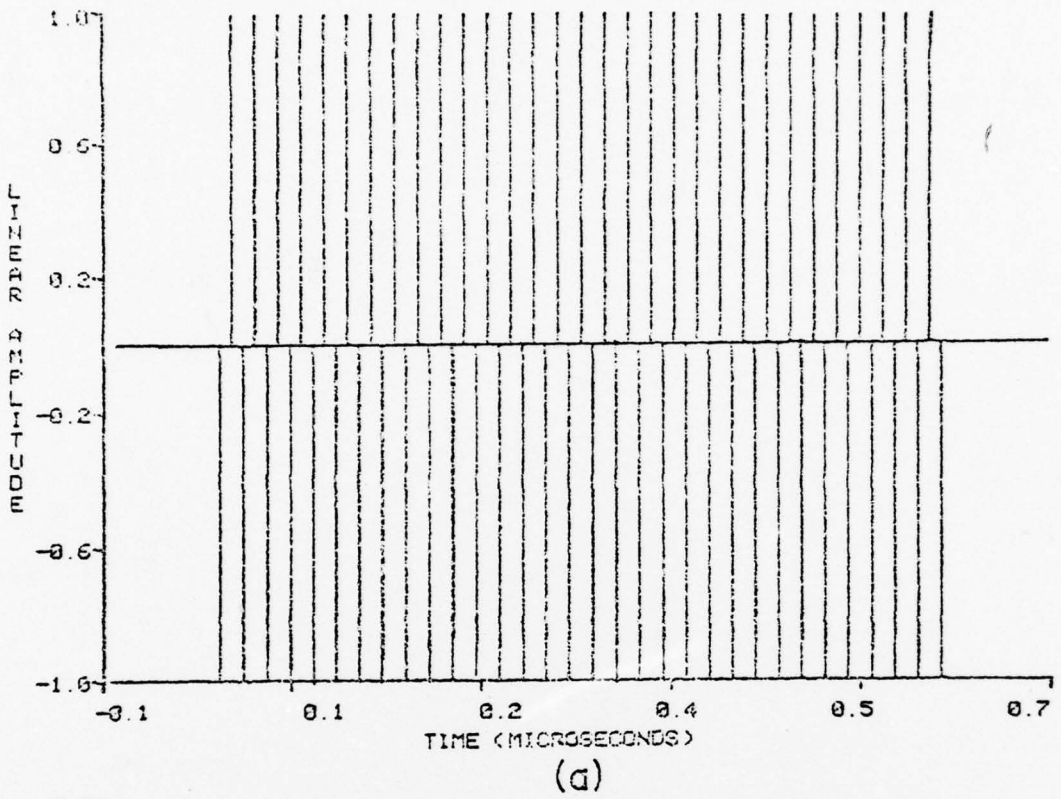

(a)

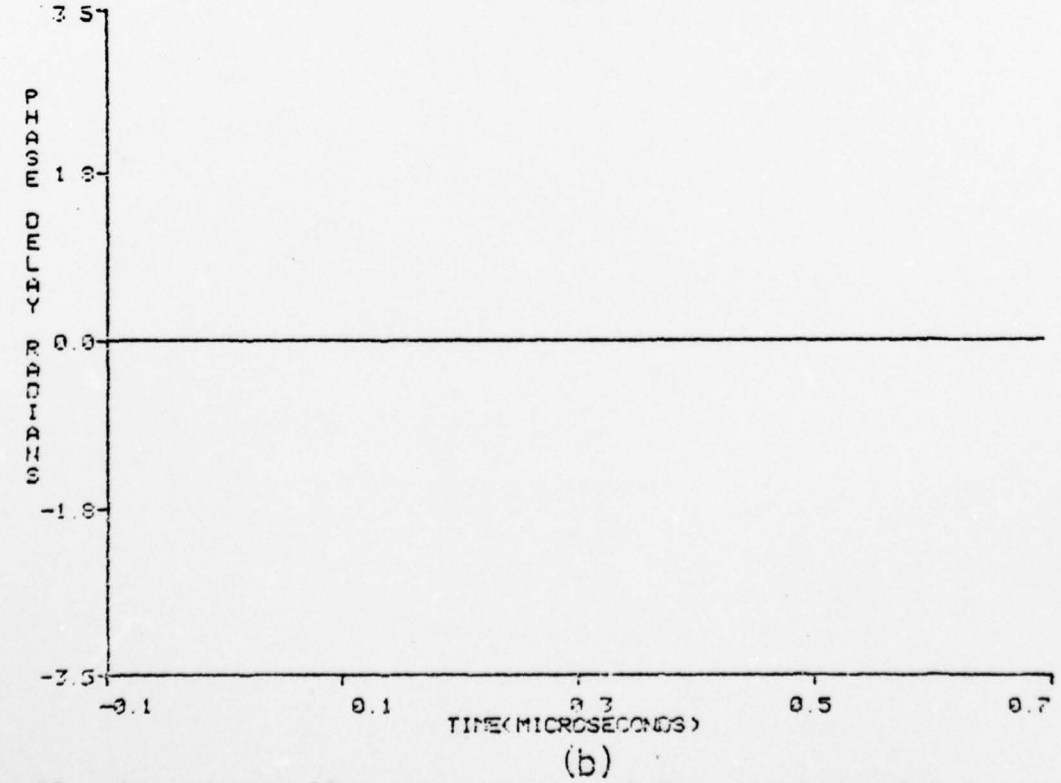

(b)

Figure 28. Non-weighted 30 tap transducer. a) Tap weights of ± 1 and b) zero tap delay.

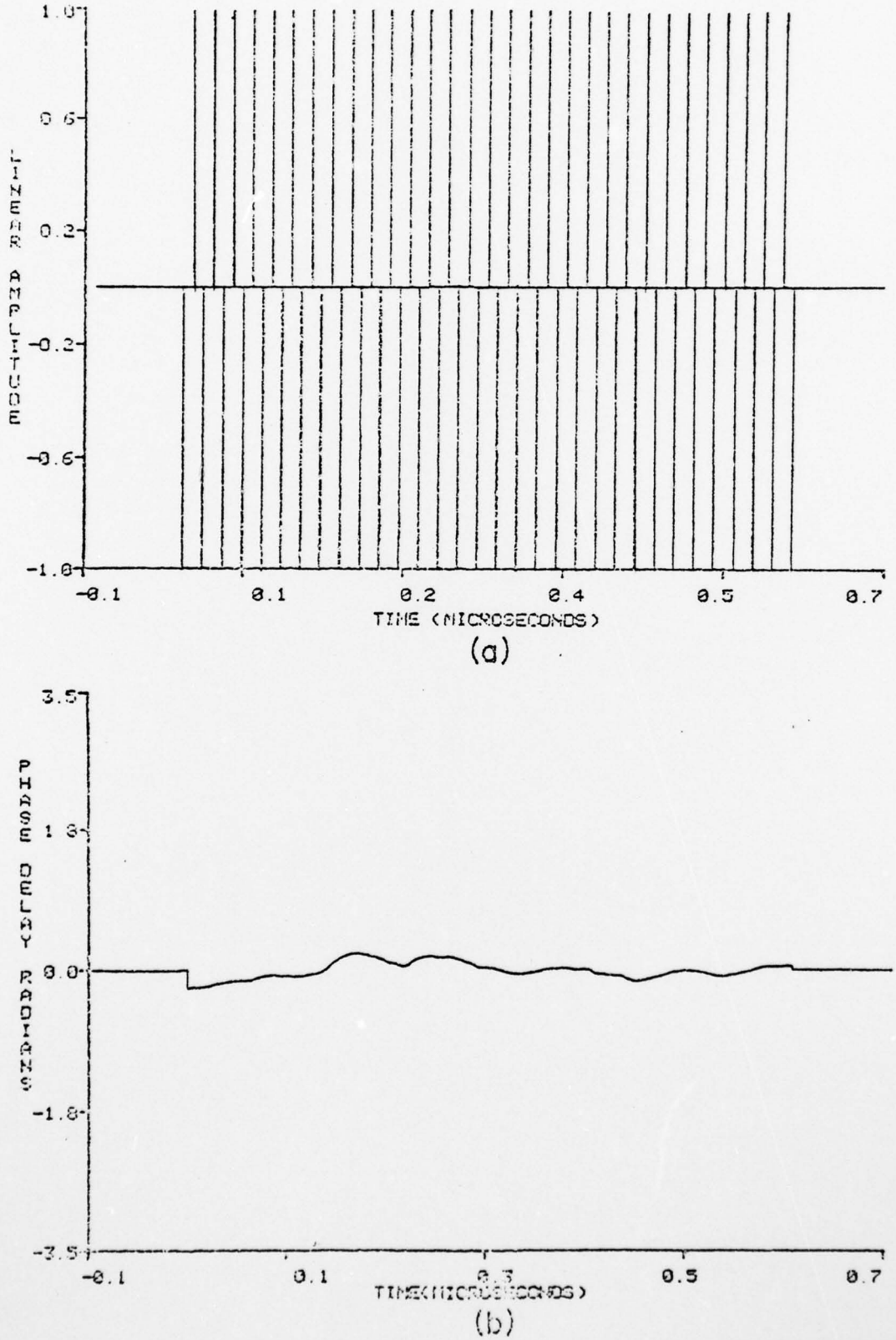

Figure 29. Non weighted 30 tap transducer. a) Tap weights of ± 1 and b) modulated tap delay based on experimental measurements.

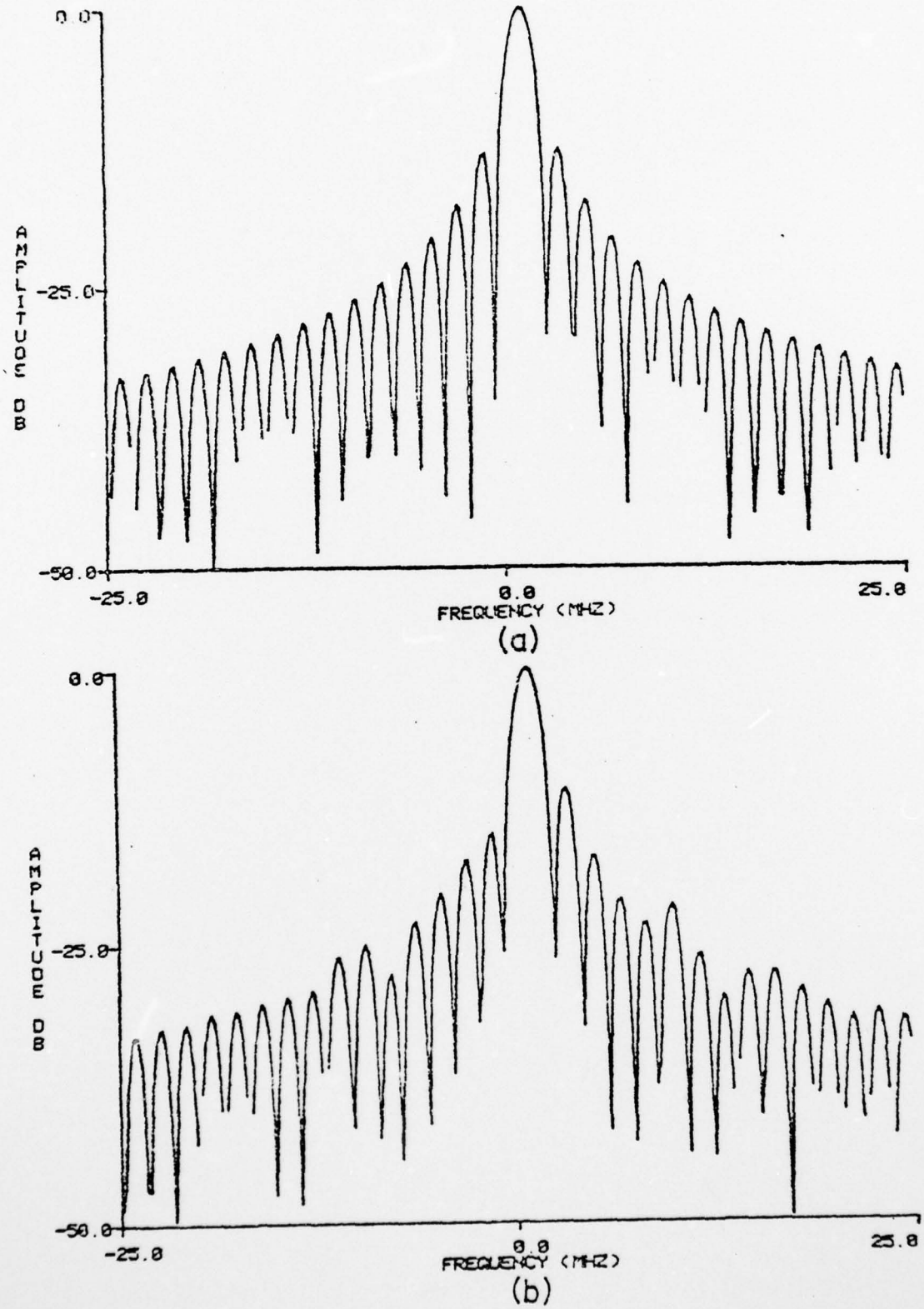

Figure 30. Frequency response of 30 tap, unweighted transducer with a) zero tap delay and b) modulated tap delay.

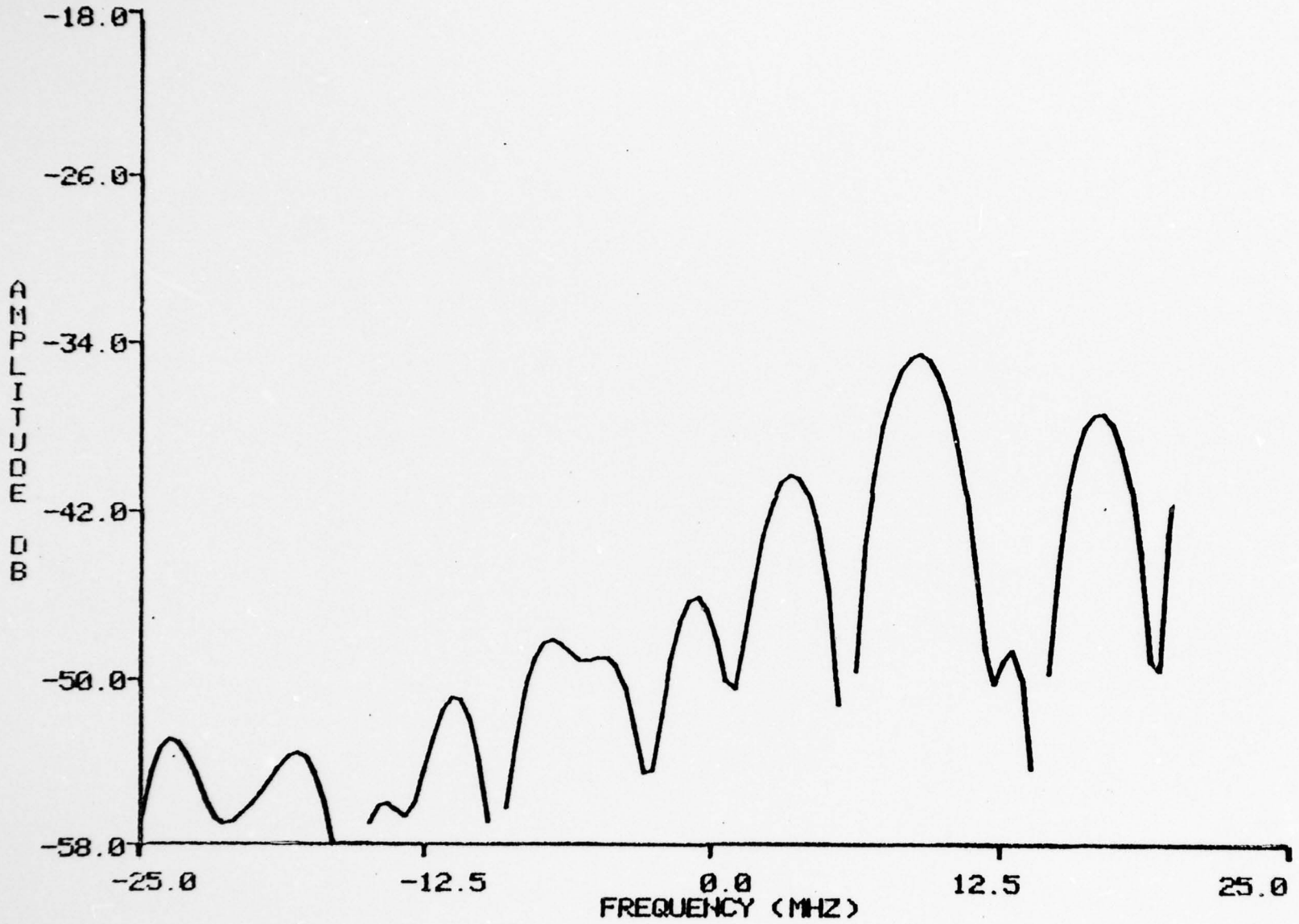

Figure 31. Frequency distortion due to tap delay errors obtained from the difference of Figures 30a and 30b.

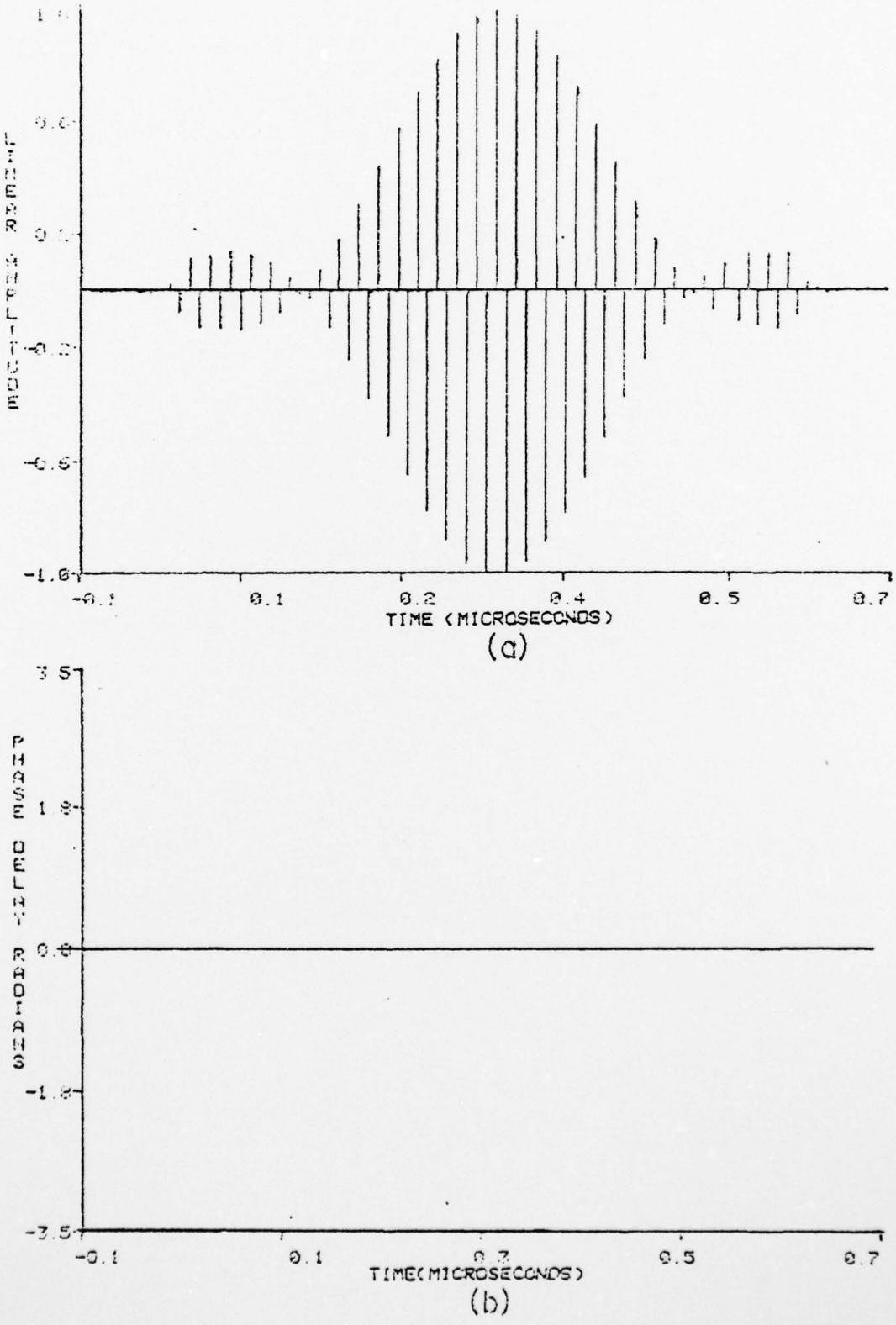

Figure 32. Specified time sampled impulse response. a) Tap weights and b) tap delay.

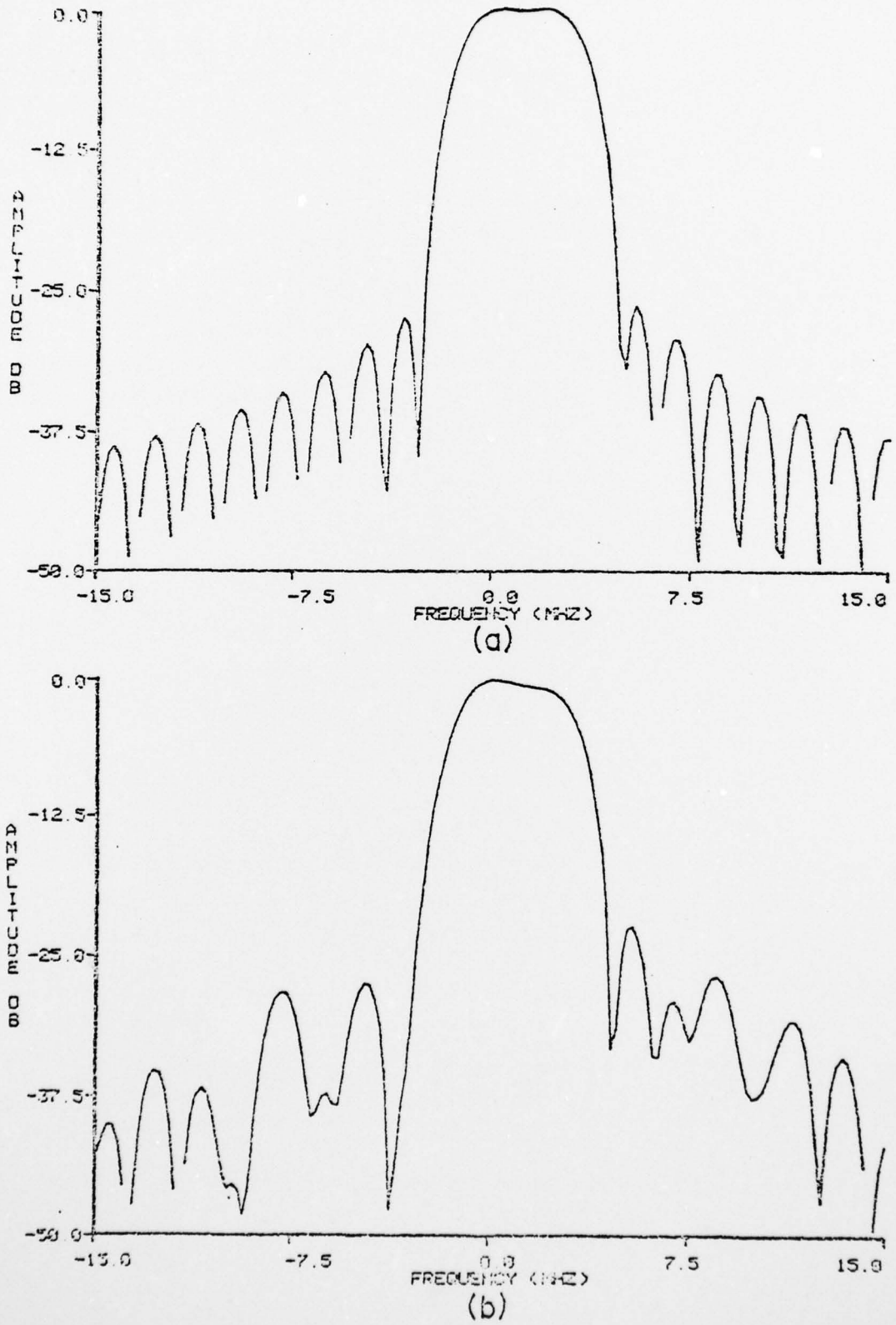

Figure 33. a) Specified frequency response and b) predicted frequency response based on measured tap delay errors.

3) Experimental Verification

To experimentally verify this analysis, a single CTWN transducer is examined using the optical laser probe [27]. Since the CTWN transducer has a uniform beam width, the complete frequency response is contained at any point in the SAW beam which eliminates scanning the beam width at various points and integrating, as is necessary for apodized devices. The TETAM testing system is used in conjunction with the optical laser probe and, with proper baseband processing procedures, 50 db or greater dynamic range is possible. The superimposed laser probe measured frequency response and the predicted response, based on the error analysis, are shown in Figure 34. The passband slope and adjacent sidelobes on the high frequency side are predicted quite well and there is a small discrepancy on the low side, however, the analysis does predict the overall trends correctly. The small discrepancies are most likely due to differences in the actual and predicted phase errors as shown in the phase envelopes of Figure 35. The rather large deviations at the 180° phase transition points is due to insufficient measurement data and should be ignored. The data match very closely in the main time lobe but deviates in the sidelobes.

A technique for the measurement of tap delay errors has been introduced and the analysis does predict the relative errors. The CTWN transducer accurately sets the tap weights and accurately predicts the measured responses when including any tap delay errors. This analysis shows that better accuracy is needed in the mask fabrication of the lower electrodes if highly selective filters are desired. The selectivity of a single transducer, at this time, is approximately 20 to 30 db, depending on the number of taps and can be substantially improved with better masks.

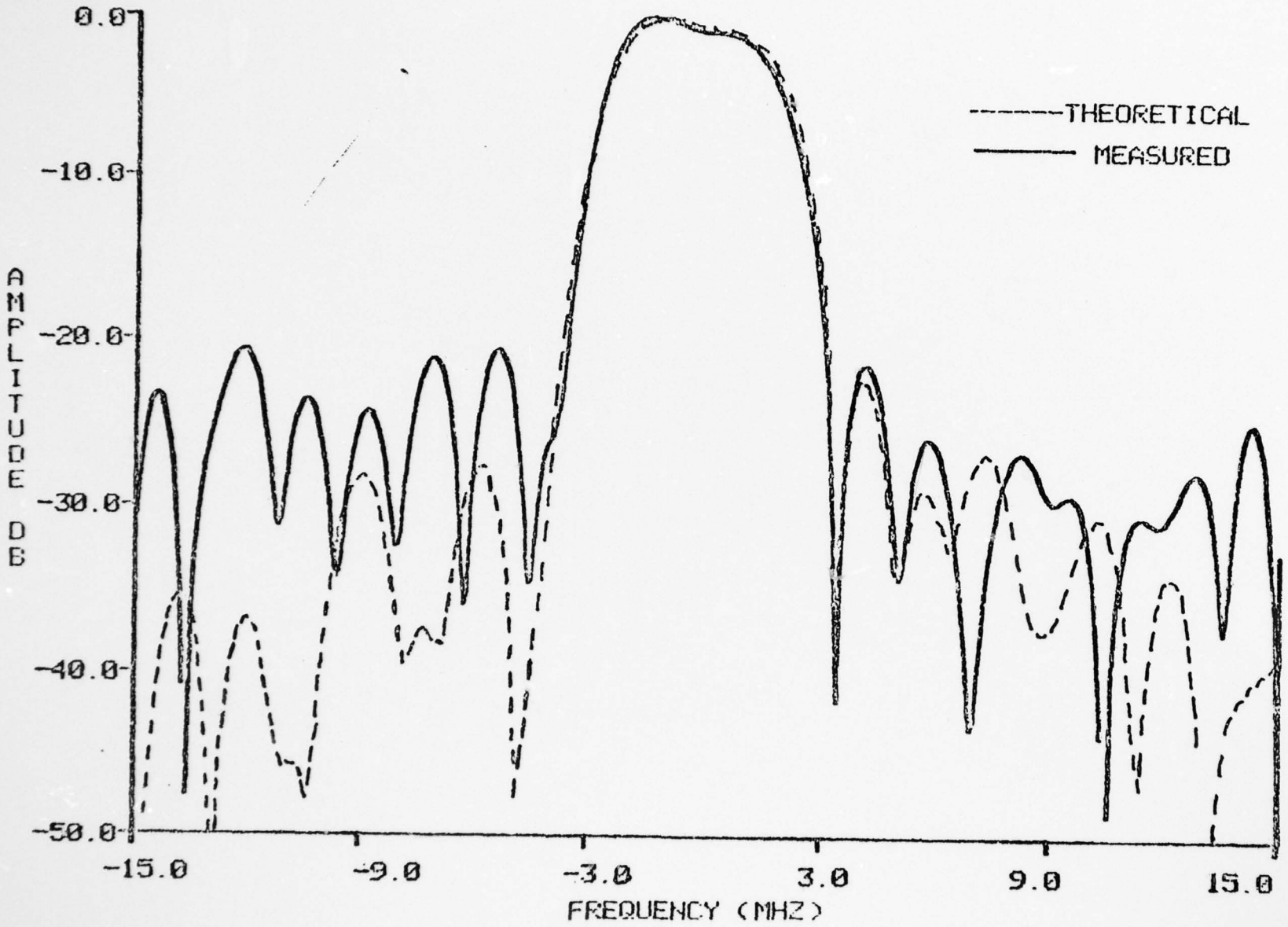

Figure 34. Predicted and measured fundamental frequency responses. Measured data obtained from laser probe.

AD-A056 199 ILLINOIS UNIV AT URBANA-CHAMPAIGN COORDINATED SCIENCE LAB F/G 9/1
CAPACITIVE TAP WEIGHT NETWORK SURFACE ACOUSTIC WAVE TRANSDUCERS--ETC(U)
MAY 77 D C MALOCHA DAAB-07-72-C-0259
UNCLASSIFIED R-780 NL

2 OF 2
AD
A056199

END
DATE
FILMED
8 -78
DDC

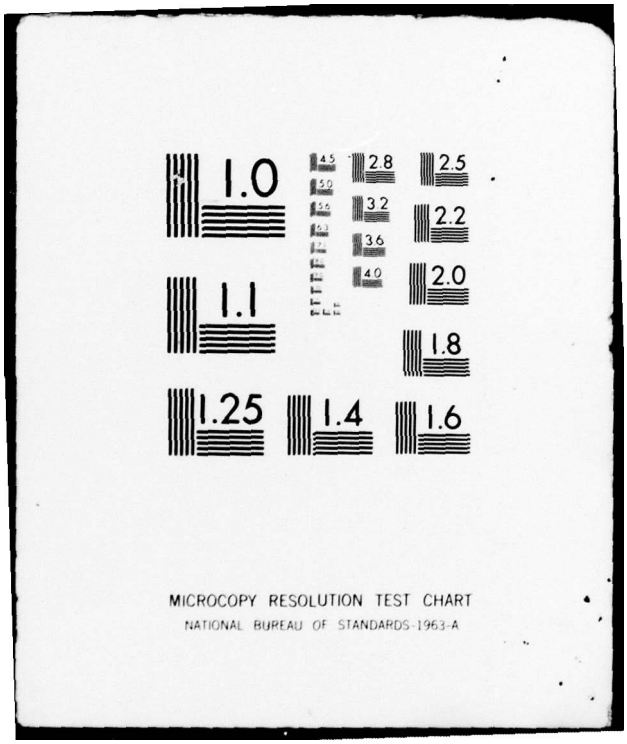
1.0
1.1
1.25
1.4
1.6
1.8
2.0
2.2
2.5
2.8
3.2
3.6
4.0
4.5
MICROCOPY RESOLUTION TEST CHART
NATIONAL BUREAU OF STANDARDS-1963-A

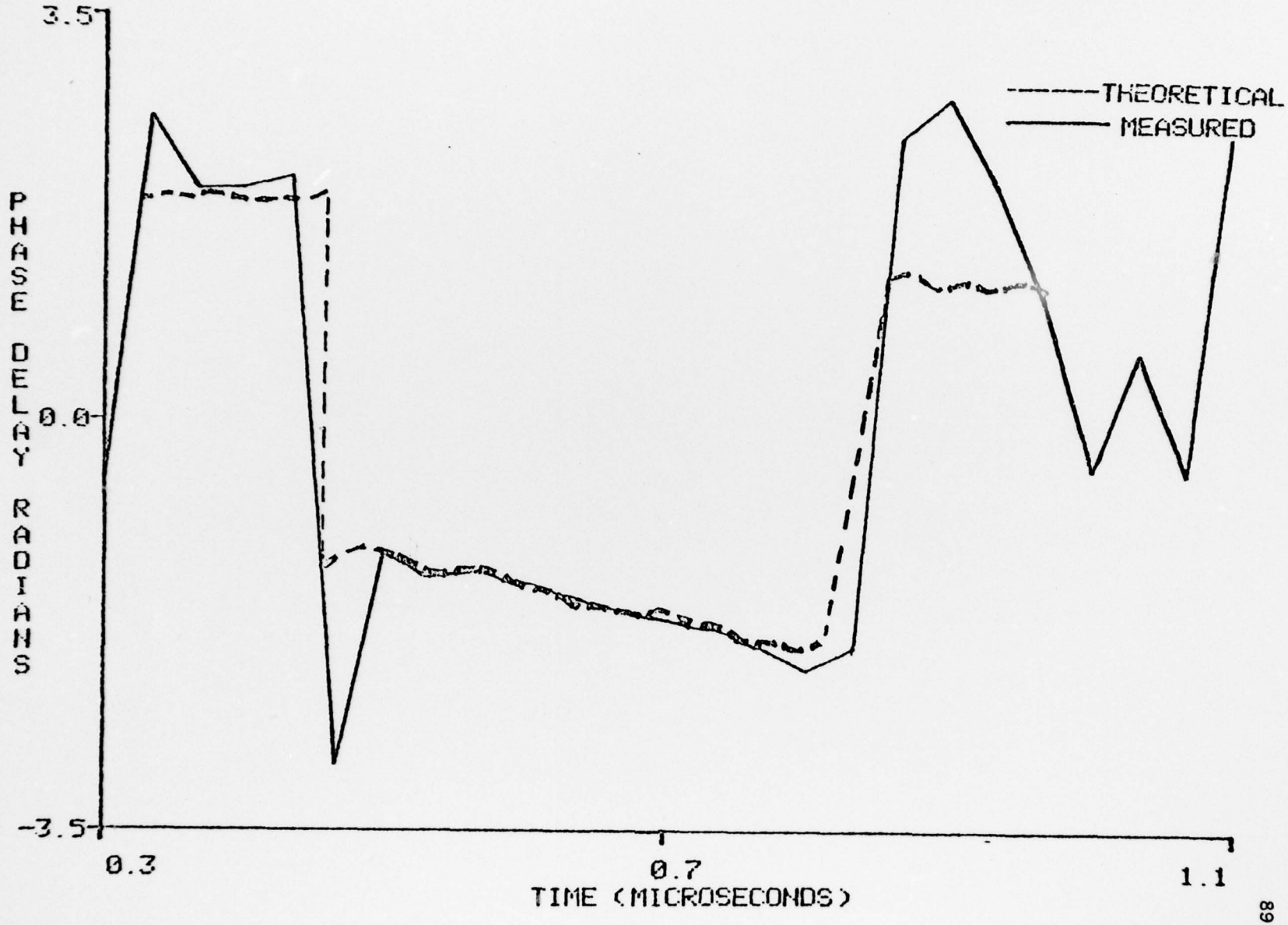

Figure 35. Predicted and measured tap delay.

LIST OF REFERENCES

1. R. M. Hayes and C. S. Hartmann, "Surface Acoustic Wave Devices for Communications," Proc. IEEE, Vol. 64, 1976, pp. 652-670.

2. D. C. Malocha and B. J. Hunsinger, "Capacitive Tap Weighted SAW Transducers," IEEE Ultrasonics Sym., Proc., 1975, pp. 411-413.

3. D. C. Malocha and B. J. Hunsinger, " Capacitive Tap Weighted SAW Transducers," IEEE Trans. on Sonics and Ultrasonics, Sept. 1977, to be published.

4. F. G. Marshall, C. O. Newton, and E. C. Paige, "Theory and Design of the Surface Acoustic Wave Multistrip Coupler," IEEE Trans., MTT-21, 1973, pp. 206-215.

5. R. S. Wagers, "Diffraction Effects in Long Narrow ID Transducers," IEEE Ultrasonics Sym. Proc., 1975, pp. 408-410.

6. R. S. Wagers, "SAW Diffraction Analysis by Paired Echo Superposition," IEEE Trans., SU-23, 1976, pp. 249-254.

7. W. J. Tanski, "Technique for Capacitive Voltage Weighting Interdigital Surface Acoustic Wave Transducers," Applied Phys. Lett., 26, 1975, 35-37.

8. R. C. Rosenfeld, et al., "Unidirectional Acoustic Surface Wave Filters with 2 db Insertion Loss," IEEE Ultrasonics Sym. Proc., 1974, pp. 425-428.

9. B. J. Hunsinger, et al., "Low Resolution Weighted Tap Transducers with Reflection and Diffraction Suppression," IEEE Ultrasonics Sym. Proc., 1975, pp. 414-417.

10. C. S. Hartmann, "Weighting Interdigital Surface Wave Transducers by Selective Withdrawal of Electrodes," IEEE Ultrasonics Sym. Proc., 1973, pp. 423-426.

11. R. H. Tancrell and M. G. Holland, "Acoustic Surface Wave Filters," Proc. IEEE, Vol. 59, 1971, pp. 393-409.

12. W. R. Smith, H. M. Gerard, and W. R. Jones, "Analysis and Design of Dispersive Interdigital Surface Wave Transducers," IEEE Trans., MTT-20, 1972, pp. 658-671.

13. C. S. Hartmann, D. T. Bell, Jr., and R. S. Rosenfeld, "Impulse Response Model Design of Acoustic Surface Wave Filters," IEEE Trans., MTT-21, 1973, pp. 162-175.

14. W. R. Smith and W. F. Pedler, "Fundamental and Harmonic Frequency Circuit Model Analysis of Interdigital Transducers with Arbitrary Metallization Ratios and Polarity Sequences," IEEE Trans., MTT-23, 1975, pp. 853-864.

15. H. Engan, "Excitation of Elastic Surface Waves by Spatial Harmonics of Interdigital Transducers," IEEE Trans., ED-16, 1969, pp. 1014-1017.

16. W. S. Jones, C. S. Hartmann, and T. D. Sturdivant, "Second Order Effects in Surface Wave Devices," IEEE Trans., SU-19, 1972, pp. 368-377.

17. C. S. Hartmann and B. G. Secrest, "End Effects in Interdigital Surface Wave Transducers," IEEE Ultrasonics Sym. Proc., 1973, pp. 413-416.

18. T. L. Szabo, K. R. Laker, and E. Cohen, "Accurate IDT Design Using Spectral Weighting," IEEE Ultrasonics Sym. Proc., 1976, pp. 543-546.

19. W. R. Smith, et al. "Analysis of Interdigital Surface Wave Transducers by Use of an Equivalent Circuit Model," IEEE Trans., MTT-17, 1969, pp. 856-864.

20. M. D. Adams and C. F. Vasile, "Experimental Verification of a New Surface Elastic Wave Bandpass Filter Synthesis Technique," IEEE Ultrasonics Sym. Proc., 1973, pp. 433-436.

21. R. W. Berry, P. M. Hall, and M. T. Harris, Thin Film Technology, Van Nostrand Reinhold Co., New York, N.Y., 1968.

22. C. M. Panasik and B. J. Hunsinger, "Precise Impulse Response Measurement of SAW Filters," IEEE Trans., SU-23, 1976, pp. 239-248.

23. K. Shibayama, et al., "Optimum Cut for Rotated Y Cut $LiNbO_3$ Crystal Used as the Substrate of Acoustic Surface Wave Filters," IEEE Proc., Vol. 64, 1976, pp. 595-597.

24. T. N. Bristol, et al., "Applications of Double Electrodes in Acoustic Surface Wave Device Design," IEEE Ultrasonics Sym. Proc. 1972, pp. 343-345.

25. B. J. Hunsinger and R. J. Kansy, "SAW Filter Sampling Techniques," IEEE Trans., SU-22, 1975, pp. 270-273.

26. D. A. Daly, et al., "Lumped Elements in Microwave Integrated Circuits," IEEE Trans., MTT-15, 1967, pp. 713-721.

27. R. Adler, A. Korpel, and P. Desmares, "An Instrument for Making Surface Waves Visible," IEEE Trans., SU-15, 1968, pp. 157.

VITA

Donald Chester Malocha was born October 17, 1950, in Chicago, Illinois. He attended Notre Dame High School in Niles, Illinois and upon graduation enrolled at the University of Illinois at Urbana-Champaign where he completed his Bachelor of Science degree in Electrical Engineering/ Computer Science in June 1972. He received a Master of Science degree in Electrical Engineering in July 1974. During his graduate study, he has held positions as teaching assistant, instructor and research assistant. He is co-author of "Capacitive Tap Weighted SAW Transducers," (with Bill J. Hunsinger) and a member of IEEE.